



# Maastricht antiarrhythmic drug evaluator (MANTA): A computational tool for better understanding of antiarrhythmic drugs



Henry Sutanto<sup>a</sup>, Lian Laudy<sup>a</sup>, Michael Clerx<sup>b</sup>, Dobromir Dobrev<sup>c</sup>, Harry J.G.M. Crijns<sup>a</sup>, Jordi Heijman<sup>a,\*</sup>

<sup>a</sup> Department of Cardiology, CARIM School for Cardiovascular Diseases, Maastricht University PO Box 616, 6200 MD, Maastricht, the Netherlands

<sup>b</sup> Computational Biology, Department of Computer Science, University of Oxford, Oxford, OX1 3QD, United Kingdom

<sup>c</sup> Institute of Pharmacology, West German Heart and Vascular Center, University Duisburg-Essen, 45122, Essen, Germany

## ARTICLE INFO

### Keywords:

Computational modeling  
Arrhythmia  
Antiarrhythmic drug  
Electrophysiology  
Cardiovascular diseases  
Heart rhythm

## ABSTRACT

Cardiac arrhythmias are a global health burden, contributing significantly to morbidity and mortality worldwide. Despite technological advances in catheter ablation therapy, antiarrhythmic drugs (AADs) remain a cornerstone for the management of cardiac arrhythmias. Experimental and translational studies have shown that commonly used AADs exert multiple effects in the heart, the manifestation of which strongly depends on the exact experimental or clinical conditions. This diversity makes the optimal clinical application of AADs challenging.

Here, we present a novel computational tool designed to facilitate a better understanding of the complex mechanisms of action of AADs (the Maastricht Antiarrhythmic Drug Evaluator, MANTA). In this tool, we integrated published computational cardiomyocyte models from different species (mouse, guinea pig, rabbit, dog, and human), regions (atrial, ventricular, and Purkinje cells) and disease conditions (atrial fibrillation- and heart failure-related remodeling). Subsequently, we investigated the effects of clinically available AADs (Vaughan-Williams Classes I, III, IV and multi-channel blockers) on action potential (AP) properties and the occurrence of proarrhythmic effects such as early afterdepolarizations. Steady-state drug effects were simulated based on a newly compiled overview of published  $IC_{50}$  values for each cardiac ion channel and by integrating state-dependent block of the cardiac  $Na^+$ -current by Class I AADs using a Markov-model approach. Using MANTA, we demonstrated and characterized important species-, rate-, cell-type-, and disease-state-specific AAD effects, including 1) a stronger effect of Class III AADs in large mammals than in rodents; 2) a rate-dependent decrease in upstroke velocity with Class I AADs and reverse rate-dependent effects of Class III AADs on action potential duration; 3) ventricular-predominant effects of pure  $I_{Kr}$  blockers; 4) preferential reduction in atrial AP upstroke velocity with vernakalant; and 5) excessive AP prolongation with Class III AADs other than amiodarone under heart failure conditions.

In conclusion, the effects of AADs are highly complex and strongly dependent on the experimental or clinical conditions. MANTA is a powerful and freely available tool reproducing a wide range of AAD characteristics that enables analyses of the underlying ionic mechanisms. Use of MANTA is expected to improve our understanding of AAD effects on cellular electrophysiology under a wide range of conditions, which may provide clinically-relevant information on the safety and efficacy of AAD treatment.

**Abbreviations:** AAD, antiarrhythmic drug; AF, atrial fibrillation; AP, action potential; APD, action potential duration; cAF, long-standing persistent ('chronic') atrial fibrillation; CaT,  $Ca^{2+}$ -transient; CiPA, comprehensive in vitro proarrhythmia assay; EAD, early after-depolarization; Endo, endocardium; Epi, epicardium; ERP, effective refractory period; FDA, U.S. food and drug administration; HCN, hyperpolarization-activated cyclic nucleotide-gated; HF, heart failure;  $IC_{50}$ , half-maximal inhibitory concentration; LV, left ventricle; MANTA, Maastricht ANTIarrhythmic drug evaluator; Mid, midmyocardium; RA, right atrium; TRP, transient receptor potential

\* Corresponding author.

E-mail addresses: [henry.sutanto@maastrichtuniversity.nl](mailto:henry.sutanto@maastrichtuniversity.nl) (H. Sutanto), [l.laudy@student.maastrichtuniversity.nl](mailto:l.laudy@student.maastrichtuniversity.nl) (L. Laudy), [michael.clerx@cs.ox.ac.uk](mailto:michael.clerx@cs.ox.ac.uk) (M. Clerx), [Dobromir.Dobrev@uk-essen.de](mailto:Dobromir.Dobrev@uk-essen.de) (D. Dobrev), [hjgm.crijns@mumc.nl](mailto:hjgm.crijns@mumc.nl) (H.J.G.M. Crijns), [jordi.heijman@maastrichtuniversity.nl](mailto:jordi.heijman@maastrichtuniversity.nl) (J. Heijman).

<https://doi.org/10.1016/j.phrs.2019.104444>

Received 17 April 2019; Received in revised form 10 July 2019; Accepted 3 September 2019

Available online 04 September 2019

1043-6618/ © 2019 The Authors. Published by Elsevier Ltd. This is an open access article under the CC BY-NC-ND license (<http://creativecommons.org/licenses/by-nc-nd/4.0/>).

## 1. Introduction

Cardiovascular diseases are the leading cause of death and disability worldwide, with cardiac arrhythmias significantly contributing to cardiovascular deaths [1]. Despite advances in catheter ablation therapy, antiarrhythmic drugs (AADs) remain widely used for the treatment of arrhythmias. However, currently available AADs have limited efficacy and important safety limitations, notably an increased risk of ventricular proarrhythmia and extra-cardiac toxicity [2–4]. Traditionally, AADs have been classified into Vaughan Williams Classes I–IV, targeting  $\text{Na}^+$ -channels,  $\beta$ -adrenoceptors,  $\text{K}^+$ -channels and L-type  $\text{Ca}^{2+}$ -channels for Classes I, II, III and IV, respectively. However, experimental and translational research performed over the last 30 years has revealed that most AADs exert effects on multiple molecular targets and alternative classifications have been developed [5–7]. In addition, the effects of AADs strongly depend on experimental/clinical conditions. For example, AADs exhibit species-dependent effects due to the distinct contribution of ion currents to the cardiac action potential (AP) across species [8], which hinder the clinical translation of animal studies [9]. Moreover, many AADs block ion channels in a rate- (or use-) dependent manner [10,11]. Some AADs (e.g. vernakalant and ranolazine) have preferential effects on atrial versus ventricular cardiomyocytes by targeting ion channels that are only expressed in the atria or preferentially inhibiting atrial  $\text{Na}^+$ -channels through state-selective blocking properties [12]. Finally, disease-related remodeling can also influence the effects of AADs. These condition-dependent effects make a detailed understanding of the clinical efficacy of AADs highly challenging and contribute to the suboptimal use of currently available AADs under dynamic clinical conditions. Moreover, such effects may hinder the development of novel, more effective and safer AADs.

Computational models can integrate experimental and pharmacological findings, and provide perfect control and observability of parameters, enabling *in silico* experiments in a controlled setting [13–15]. Several software tools have been developed to enhance the understanding of cardiovascular (patho) physiology, ranging from cellular electrophysiology to hemodynamics in the entire cardiovascular system [15]. For example, the CircAdapt® model simulates cardiovascular mechanics and hemodynamics to study (patho)physiology of heart and circulation [16] and ECGSIM solves the forward problem of electrocardiology to compute electrograms at the body surface that result from user-defined electrical activity at the heart surface [17]. Both have also been used for educational purposes. However, to simulate AAD effects, detailed models of cardiac cellular electrophysiology are needed. Several relatively user-friendly tools have been developed to simulate cardiac cellular electrophysiology [18–22]. However, these tools often focus on a single model and are limited in their ability to compare (state-dependent) AAD effects. Thus, despite the relevance of understanding the complex effects of AADs under various conditions, there is, to the best of our knowledge, no software tool available that addresses this critical issue.

Here, we present a novel, user-friendly software tool (the Maastricht Antiarrhythmic Drug Evaluator; MANTA) that enables analyses of species- and condition-dependent effects of a wide range of clinically relevant AADs on cardiac ion currents, as well as their downstream effects on AP and  $\text{Ca}^{2+}$ -transient (CaT) properties (Fig. 1). MANTA may facilitate a better understanding of the complex effects of AADs, thereby promoting improved use of these drugs during experiments as well as increased awareness of their limitations under specific clinical conditions. Finally, it can provide insight into the proarrhythmic side-effects of some AADs. In addition to its research use, MANTA can be employed to teach students about the mechanism-of-action of currently available AADs.

## 2. Methods

### 2.1. The Maastricht antiarrhythmic drug evaluator (MANTA)

MANTA was developed as an extension of Myokit, a python-based software tool designed for cardiac AP simulations [23]. MANTA integrates a wide range of published cardiomyocyte models and AADs (based on their affinity for different cardiac ion channels, including state-dependent block of  $\text{Na}^+$ -channels, as detailed below). A graphical user interface was created, which provides easy access to settings, enabling simulations of AAD effects under different conditions. A Python package was generated to facilitate installation of MANTA from the Python Package Index (PyPI) on Microsoft Windows-based platforms. MANTA and Myokit are both freely available and can be downloaded from the authors' websites (<http://www.jordiheijman.net> and <http://www.myokit.org>). Detailed installation instructions are provided in the Online Supplement.

MANTA displays simulation results of two *in silico* cardiomyocyte models side-by-side (Fig. 2A). By default, the AP and CaT are shown for both models, but drop-down lists enable visualization of all model variables, including intracellular ion concentrations and ion currents. Simulation of up to two clinically available AADs at user-defined concentrations enables comparison of the electrophysiological effects of these agents. In “custom” mode, the activity of individual ion channels can be adjusted to study the effect of these changes on the AP, enabling simulations of novel AADs. Moreover, in the “options” panel, several properties of the experimental environment can be adjusted (Fig. 2B), including the number of pre-paced beats, pacing frequency and extracellular ionic concentrations ( $[\text{K}^+]_o$ ,  $[\text{Na}^+]_o$ , and  $[\text{Ca}^{2+}]_o$ ). The AP duration (APD), maximum AP upstroke velocity ( $dV/dt_{\max}$ ) and CaT amplitude are automatically calculated for each model and condition. MANTA also enables the user to perform an  $S_1S_2$  protocol simulation to calculate the frequency-dependent effective refractory period (ERP), which is defined as the shortest interval after the start of the last stimulus allowing the generation of a new AP. We considered a new AP to be generated when maximal membrane potential after 75% of the current  $\text{APD}_{90}$  exceeded 80% of the peak of the current AP. Since this threshold may not be appropriate for all models and/or stimuli, manual confirmation of ERP detection is recommended. Subsequently, the results can be exported as comma-separated value (.csv) or text (.txt) files for further analysis (Fig. 2B).

### 2.2. Incorporation of computational models of cardiac cellular electrophysiology

To investigate the effects of AADs at the cellular level, 17 previously published and validated *in silico* cardiomyocyte models [24–35], reflecting different species, regions of the heart and disease-related remodeling, were incorporated into MANTA. Each model contains a number of ion currents and transporters with various degrees of complexity, ranging from basic Hodgkin-Huxley mathematical models to more complex Markov models. An overview of the computational cardiomyocyte models is provided in Table 1. It is possible to add additional cardiomyocyte models to MANTA using the instructions provided in the Online Supplement.

### 2.3. AADs available in the current version of MANTA

In total, 25 AADs belonging to Vaughan-Williams Classes I, III and IV, and exhibiting diverse cardiac ion-channel-blocking properties were included in MANTA (Table 2). AADs commonly used in clinical practice (flecainide, amiodarone) as well as more recent multi-channel blockers (e.g., vernakalant), were incorporated, but Class II AADs ( $\beta$ -blockers) were excluded from the tool due to the absence of  $\beta$ -adrenoceptor-signaling components in most of the available cardiomyocyte models. To model the effect of an AAD on a cardiac ion channel, its maximal

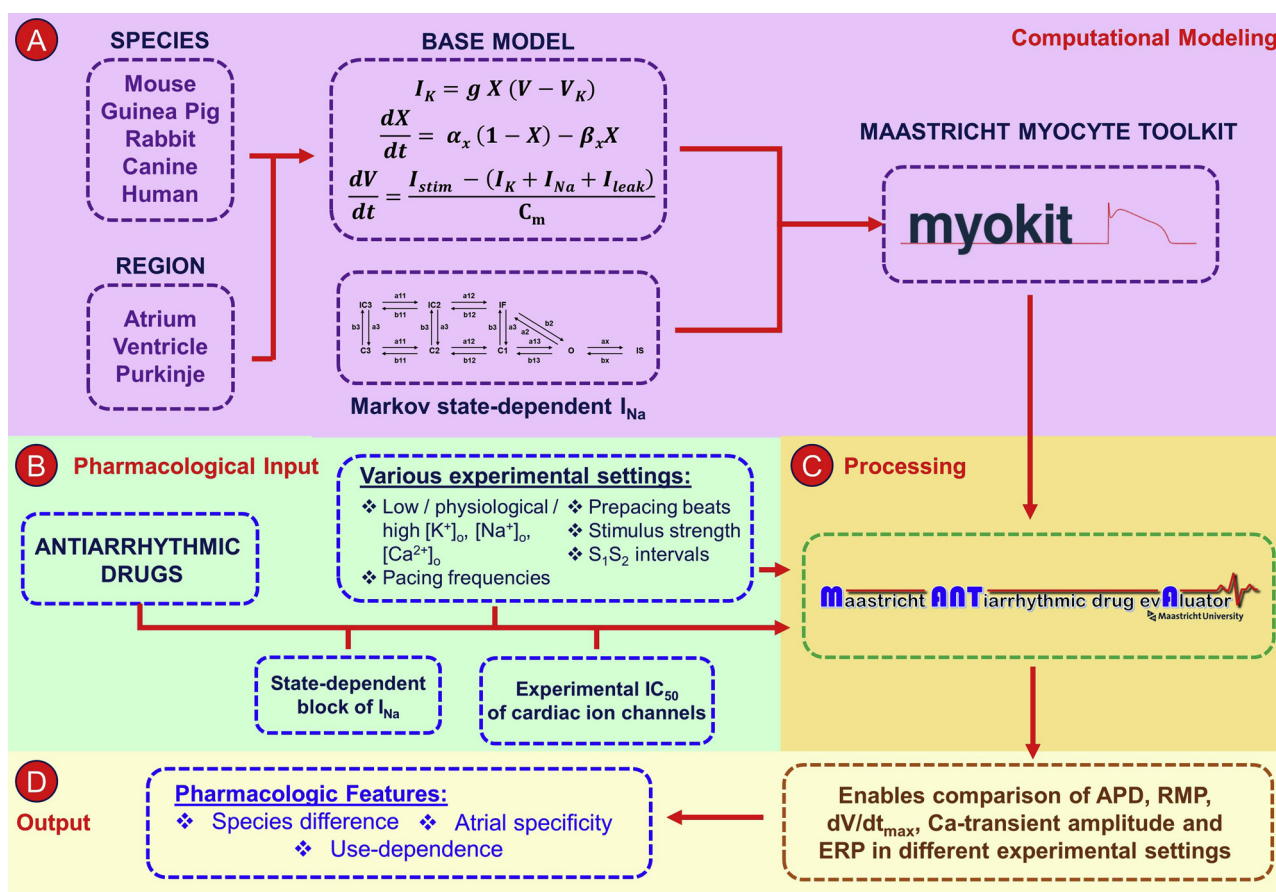


**Fig. 1.** Maastricht Antiarrhythmic Drug Evaluator (MANTA) and its components. MANTA is developed as an extension of Myokit, a software tool designed for cardiac action potential (AP) simulations [23]. MANTA enables analyses of the effects of antiarrhythmic drugs (AADs) on the AP under user-defined experimental settings by integrating a large number of *in silico* cardiomyocyte models of various species with a newly compiled overview of pharmacodynamic properties of AADs from different Vaughan-Williams Classes. APD: action potential duration, RMP: resting membrane potential,  $dV/dt_{max}$ : upstroke velocity, ERP: effective refractory period,  $IC_{50}$ : half-maximal inhibitory concentration;  $I_{Na}$ :  $Na^+$  current.

conductance was scaled based on the given drug concentration and a sigmoidal Hill curve based on previously reported 50% inhibitory concentrations ( $IC_{50}$ ), as summarized in Table 2. Validation of each drug based on an overview of published  $IC_{50}$  values and dose-response curves is provided in Supplemental Table 1 and Supplemental Fig. 1A–X. Moreover, based on these  $IC_{50}$  values, AAD-induced changes in APD were largely consistent with experimental data in most models (Supplemental Fig. 2).

#### 2.4. Incorporation of state-dependent $Na^+$ -current block in cardiomyocyte models

Since Class I AADs have markedly different affinities for individual states of the  $Na^+$ -channel (open, closed, and inactivated) [36–38], we introduced a state-of-the-art  $Na^+$ -channel Markov model enabling simulation of state-dependent  $Na^+$ -channel block (Supplemental Fig. 3) [36] in each of the 17 cardiomyocyte models. The parameters of the baseline  $Na^+$ -current ( $I_{Na}$ ) Markov models were optimized to produce similar peak amplitude, non-inactivating late current, voltage dependence of activation and inactivation, time constants of inactivation and recovery from inactivation of  $I_{Na}$ , along with upstroke velocity during current-clamp simulations as the original Hodgkin-Huxley models in the absence of AADs. Details of the  $I_{Na}$  Markov model and the results of the optimization procedure are provided in Supplemental Figs. 3–4.

The baseline Markov model was extended with drug-blocked states for neutral and charged fractions of Class I AADs, which have distinct affinities for open, closed and inactivated states (Supplemental Fig. 3)

[36]. In line with the approach by Moreno et al. [36], the parameters representing the affinities of flecainide and lidocaine for open, closed and inactivated states were fixed and parameters reflecting state transitions within blocked states were subsequently numerically optimized to reproduce experimentally observed drug-block properties for individual baseline  $I_{Na}$  Markov models (Supplemental Table 2). In particular, drug-induced shifts in steady-state availability, tonic block and rate-dependent block at 5 Hz for various AAD concentrations, as well as frequency dependence from 1 to 10 Hz and recovery from rate-dependent block by flecainide and lidocaine could be reproduced using this Markov model (Supplemental Fig. 5). Parameters for vernakalant were similarly optimized to reproduce the tonic, rate-dependent and voltage-dependent block observed in experimental studies [39].

### 3. Results

#### 3.1. Species differences in AAD effects

Numerous animal models have been used to study AADs and species differences in AAD effects may hinder the clinical translation of experimental findings [40]. Therefore, we investigated the species-dependent effects of AADs on the APs of mouse, guinea pig, rabbit, dog and human left ventricular (LV) cardiomyocyte models using MANTA. Application of the Class Ic AAD flecainide resulted in a concentration-dependent prolongation of APD and reduction in  $dV/dt_{max}$  in all species. However, the extent of APD prolongation and  $dV/dt_{max}$  reduction were species dependent, with the largest APD prolongation in the

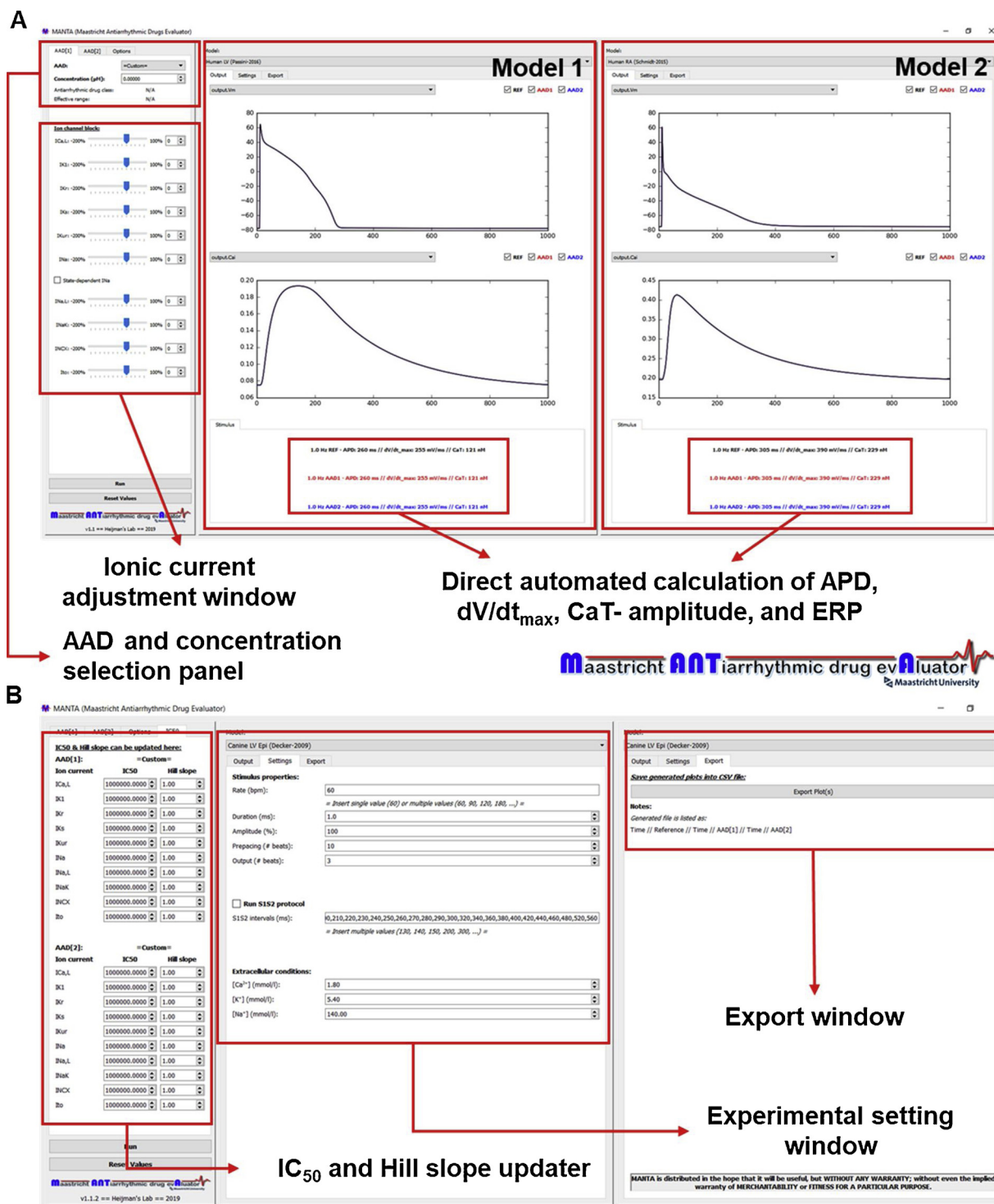


**Fig. 2.** The MANTA graphical user interface. MANTA displays two cardiomyocyte models side-by-side and enables comparison of up to two AADs at a user-defined concentration. **A)** Main MANTA screen, comparing the simulation results of two different computational models side-by-side, whilst automatically calculating the APD,  $dV/dt_{\max}$ , and  $Ca^{2+}$ -transient amplitude. **B)** Additional tabs in the MANTA interface enabling alterations in simulation settings (including pacing frequency and different extracellular ionic concentrations), alterations in the  $IC_{50}$  and/or Hill coefficients of the selected drug for each ion-channel target, as well as allowing users to export the simulation results to comma-separated values (csv) files for further analysis or data extraction.

Passini human LV cardiomyocyte model (29% increase with 1  $\mu$ M and 72% increase with 3  $\mu$ M flecainide) and the smallest APD prolongation in the Faber guinea pig LV and Mahajan rabbit LV model (+5% with 1  $\mu$ M and +9% with 3  $\mu$ M). On the other hand, the biggest reduction of  $dV/dt_{\max}$  was achieved by the Faber guinea pig LV model (51 mV/ms (−14%) and 116 mV/ms reduction (−32%) with 1  $\mu$ M and 3  $\mu$ M

flecainide; Fig. 3A).

Similarly, the effects of dofetilide, a Class III AAD with primarily  $I_{Kr}$ -blocking properties, were highly species dependent. Low (6 nM) and high (12 nM) concentrations of dofetilide did not prolong APD in the Bondarenko mouse LV model (Fig. 3B) and produced minor prolonga- tion in the Faber guinea pig LV model (+7% and +11%) and the

**Table 1**

**The computational cardiomyocyte models available in MANTA.** LV: left ventricle, RA: right atrium, Endo: Endocardium, Mid: Midmyocardium, Epi: Epicardium, HF: heart failure, cAF: long-standing persistent ('chronic') atrial fibrillation.

No	Species	Region	First Author	Year	Citation
1	Mouse	LV	Bondarenko	2004	[24]
2	Guinea Pig		Luo	1991	[25]
3			Faber	2000	[26]
4	Rabbit		Mahajan	2008	[27]
5	Canine		Decker	2009	[28]
6			Heijman	2011	[29]
7	Human	LV (Endo)	O'Hara	2011	[30]
8			Passini	2016	[31]
9		LV(Mid)	O'Hara	2011	[30]
10		LV (Epi)	O'Hara	2011	[30]
11		HF LV (Endo)	Passini	2016	[31]
12		RA	Courtemanche	1998	[32]
13			Schmidt	2015	[33]
14		cAF RA	Courtemanche	1998	[32]
15			Schmidt	2015	[33]
16		Purkinje	Stewart	2009	[34]
17			Sampson	2010	[35]

Mahajan rabbit LV model (+5% and +8%). In dog and human models, the same concentrations of dofetilide led to a much larger APD prolongation, with 38% and 84% increase in APD in the Passini human LV model and the occurrence of proarrhythmic EADs in the Decker canine LV model with 12 nM dofetilide. No change in  $dV/dt_{max}$  was observed

**Table 2**

**List of AADs and their  $IC_{50}$  values (in  $\mu M$ ) and Hill coefficients for individual drug targets incorporated into MANTA.** In total, MANTA includes 25 AADs, corresponding to Classes I, III and IV of the Vaughan-Williams classification, which can affect 10 major ion currents. Experimental sources and validation for these  $IC_{50}$  values are provided in the **Online Supplement**. Results are presented as  $IC_{50}$  and Hill coefficient or  $IC_{50}$  value only in case of a Hill coefficient of 1.0.

	$I_{Ca,L}$	$I_{K1}$	$I_{Kr}$	$I_{Ks}$	$I_{Kur}$	$I_{to}$	$I_{Na}$	$I_{Na,L}$	$I_{NaK}$	$I_{NCX}$
Class Ia										
Ajmaline	70		1		1.7	14	28			
Cibenzoline	20	33.7	15				15	45		
Disopyramide	1037		11			21	168.4			
Procainamide	340	33	300	810			646			
Quinidine	10		0.7	5	5	3.5	12	10		
Quinine	27		5	37		79	24	11		
								(h = 0.4)		
Class Ib										
Lidocaine							20	10.8		
Phenytoin	22.07		120				80.41			
Ranolazine	250		12	100			200	8		91
Class Ic										
Flecainide	27.1		1.6		2.9	10	6.5	20		
						(h = 0.8)		(h = 0.6)		
Propafenone	1.55		0.44	16		7.2	2.5	4		
Class III										
Ambasilide			3.6		35	23				
Acute amiodarone	1.5		3.0	100		3.8	5	9		3.4
	(h = 0.6)					(h = 0.4)		(h = 0.4)		
Chronic amiodarone	1.5		0.8	20		3.8	5	9		3.4
	(h = 0.6)		(h = 0.6)	(h = 0.6)		(h = 0.4)		(h = 0.4)		
Bepridil	2.8		0.16	6.1			2.2	1.8		
Dofetilide	26.7		0.008	415			150			
Dronedarone	4		2	10			1			
							(h = 1.7)			
E-4031			0.008							
Ibutilide	62.5		0.02				42.5			
Niferidil	100	203	0.0382	28	60	203				
Sotalol	2100	2500	100	3500			7000			
Vernakalant	84		20		15	15	90	14		
Class IV										
Diltiazem	0.45		13				22			
Nitrendipine	0.025	417	20	19.5			21.5			
Verapamil	0.2		0.5		2.2		35			

with dofetilide (Fig. 3B), consistent with  $I_{Kr}$  inhibition as primary mechanism of action.

Verapamil is a Class IV AAD ( $Ca^{2+}$ -channel blocker) with additional  $I_{Kr}$ ,  $I_{Kur}$  and  $I_{Na}$ -blocking effects [41–49]. In the Bondarenko mouse LV model, a 17% increase in APD was observed with 2.0  $\mu M$  Verapamil, while in the Faber guinea pig LV model, APD decreased by 25% and 35% with 0.4  $\mu M$  and 2.0  $\mu M$  verapamil, respectively (Fig. 3C). An APD reduction (of 60% and 73%) was also obtained in the Mahajan rabbit LV model. On the other hand, in the canine and human models, verapamil showed various degrees of APD prolongation depending on the proportional balance between  $I_{CaL}$ - and  $I_{Kr}$ -block. For example, in the Decker canine LV model, low concentrations of verapamil resulted in 42% APD prolongation, while high concentrations only slightly increased APD, with  $I_{CaL}$  inhibition offsetting APD-prolonging effects with higher concentrations of verapamil. By contrast, the Passini human LV model showed a larger APD prolongation with 2.0  $\mu M$  verapamil (+137%) compared to 0.4  $\mu M$  (+28%). These results highlight the complex concentration- and species-dependent effects of AADs.

### 3.2. Rate-dependence and reverse rate-dependence of AADs

Class I AADs have pronounced rate-dependent properties due to state-dependent  $Na^{+}$ -channel block. Most Class I AADs primarily block the  $Na^{+}$ -channel during open and inactivated states, leading to increased inhibition at faster pacing rates [10]. In the closed state, the drug unbinds, losing its ability to block the  $Na^{+}$ -channel [50,51]. At slow rates, the channel spends more time in the closed state, promoting greater drug unbinding. By contrast, Class III AADs exhibit the strongest

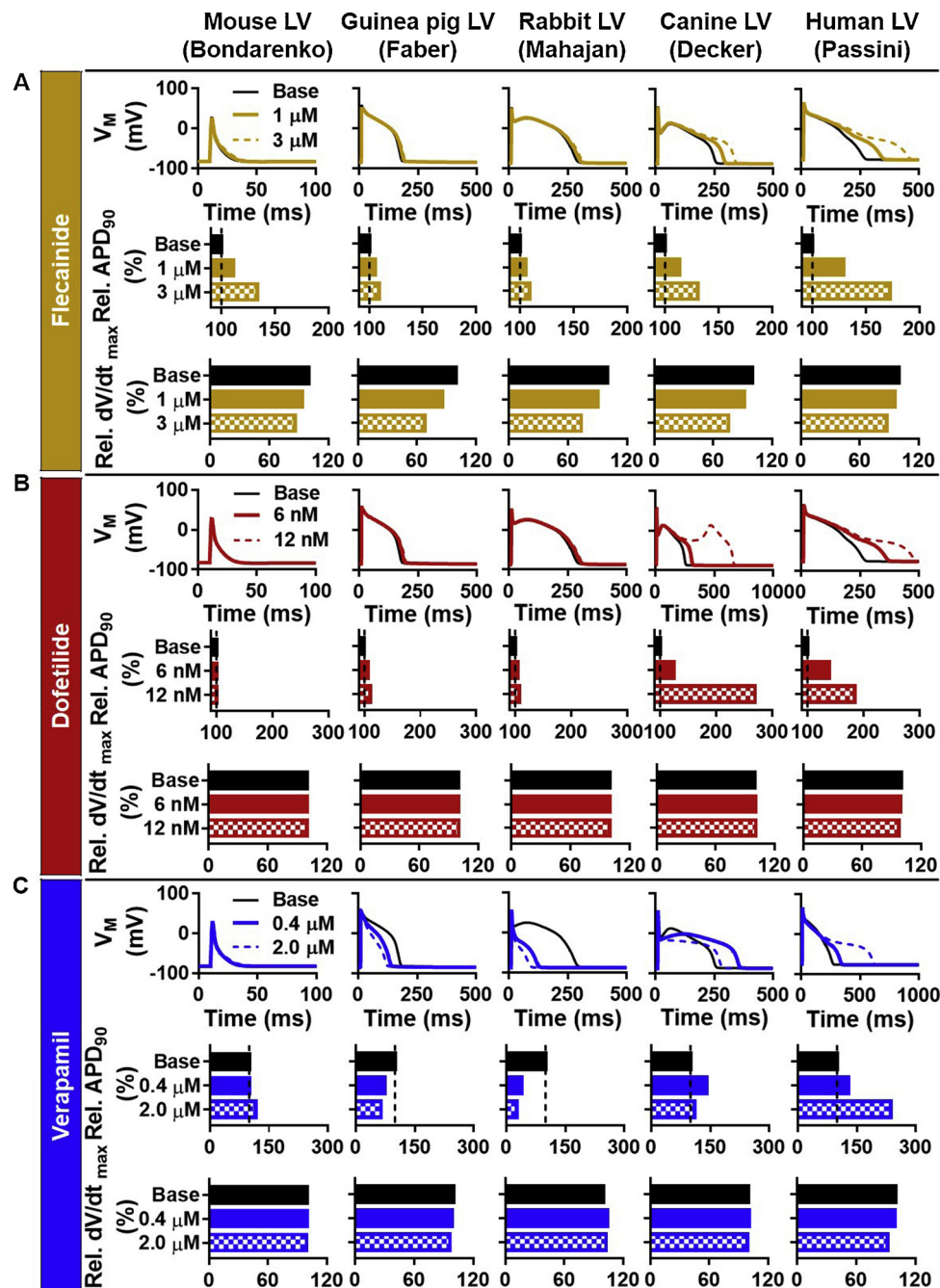


**Fig. 3.** The effects of flecainide, dofetilide and verapamil on action potential (AP) duration (APD) and upstroke velocity ( $dV/dt_{max}$ ) of various species. A) APs at baseline and with 1 and 3  $\mu M$  flecainide (top) and quantification of APD and  $dV/dt_{max}$  changes relative to baseline (bottom) for mouse, guinea pig, rabbit, dog and human left-ventricular (LV) cardiomyocyte models. B) Similar to panel A for baseline, 6 nM and 12 nM dofetilide. C) Similar to panel A for 0.4  $\mu M$  and 2.0  $\mu M$  verapamil.

APD-prolonging effect at slow rates, a concept termed reverse rate-dependence [10,52]. Reverse rate-dependence can potentially increase the risk of ventricular proarrhythmia, particularly during bradycardia. Several mechanisms may contribute to this property of Class III drugs, including state-dependent interactions with  $K^+$ -channels [37]; rate-dependent changes in the contribution of  $K^+$ -channels to repolarization [53], e.g., accumulation of incompletely deactivated  $I_{Ks}$  during fast pacing frequencies [10,54]; or accumulation of  $K^+$  in the sarcolemmal cleft during fast pacing, reducing the APD-prolonging effect of  $K^+$ -channel blockers [55]. Finally, reverse rate-dependence is not restricted to pacing rates, but is an intrinsic property of the AP resulting from the interaction between APD and net membrane current, whereby a fixed

reduction in membrane current results in a stronger APD-prolonging effect when the initial/baseline APD is long enough (as is the case at slow rates) [11,56].

We employed MANTA to demonstrate the (reverse) rate-dependence of Class I and III AADs in the canine and human LV cardiomyocyte models (Fig. 4). Simulated application of 3  $\mu M$  flecainide decreased  $dV/dt_{max}$  the most at higher pacing frequencies in both canine and human LV models, highlighting the rate-dependent behavior of Class I AADs. The  $I_{Kr}$ -blocking property of flecainide also resulted in prolongation of APD, which was most pronounced at slower pacing rates, consistent with the reverse rate-dependence of traditional  $I_{Kr}$ -blocking drugs (Fig. 4A and C). Together, the reverse rate-dependent APD prolongation

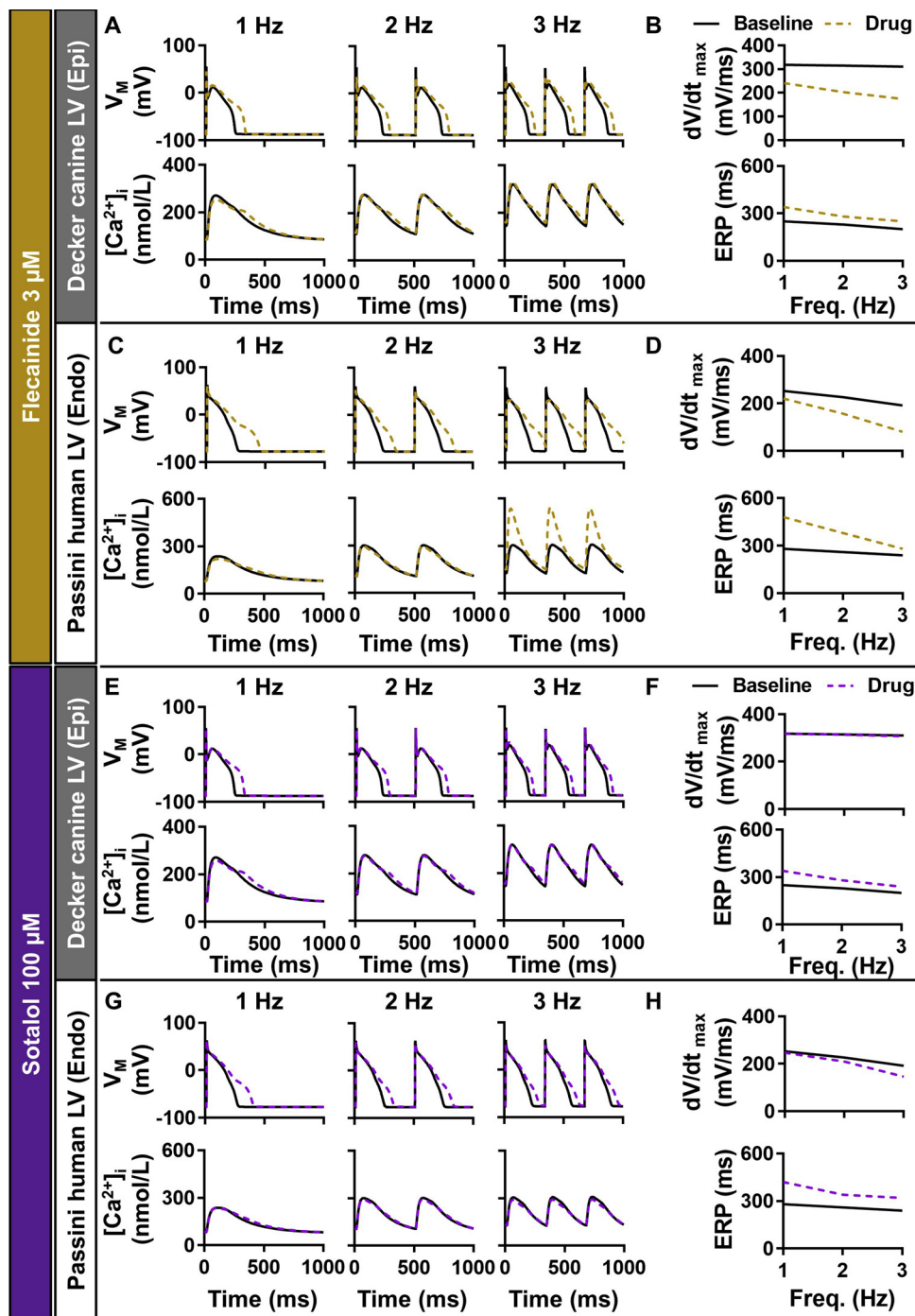


Fig. 4. The effect of flecainide and sotalol on upstroke velocity ( $dV/dt_{\max}$ ) and effective refractory period (ERP) of canine and human LV models. A–D) Action potentials and  $Ca^{2+}$ -transients during steady-state pacing at 1, 2, or 3 Hz in the absence (black solid lines) or presence (dashed lines) of  $3 \mu M$  flecainide in the Decker canine LV model (A) and Passini human LV model (C). Panels B and D show frequency dependence of  $dV/dt_{\max}$  and ERP in both models, highlighting a rate-dependent reduction in  $dV/dt_{\max}$ . E–H) Similar to panels A–D for  $100 \mu M$  sotalol, a Class III AAD, showing a reverse rate-dependence of ERP prolongation, without significant effects on  $dV/dt_{\max}$ .

and rate-dependent reduction of excitability, leading to post-repolarization refractoriness, resulted in a prolongation of ERP in both models, with the largest effect at slow pacing frequencies (Fig. 4B and D). On the other hand, simulated application of  $100 \mu M$  sotalol (simulated without  $\beta$ -blocking effects) resulted in a clear reverse rate-dependent pattern in both models, with more pronounced APD prolongation with decreasing pacing frequency (Fig. 4E–H). Sotalol did not directly affect  $dV/dt_{\max}$  in the canine model and had a minor indirect effect on  $dV/dt_{\max}$  in the human model at fast rates due to a shorting of the diastolic interval and less time for recovery from inactivation of  $I_{Na}$  (Fig. 4G–H).

### 3.3. Atrial specificity of AADs

Atrial fibrillation (AF) is the most common clinically relevant heart

rhythm disorder and despite advances in catheter ablation therapy, pharmacological management with anticoagulants and AADs remains a cornerstone for the treatment of symptomatic AF [57–59]. However, the use of currently available AADs is limited by an increased risk of ventricular proarrhythmia [60]. The development of atrial-specific AADs has been proposed to enable a safer, more effective pharmacological treatment of AF [2,12]. We employed MANTA to compare AAD effects on atrial and ventricular APs and assessed potential proarrhythmic side effects. The Class III AAD ibutilide ( $0.01 \mu M$ ) prolonged the APD of the human RA model by 27 ms (Fig. 5A), while in the human LV endocardium model, APD was increased by 68 ms at 1 Hz pacing (Fig. 5B), suggesting a ventricular-predominant effect with associated risk for drug-induced “torsade-de-pointes” arrhythmias. On the other hand, vernakalant has been shown to exhibit atrial predominant effects

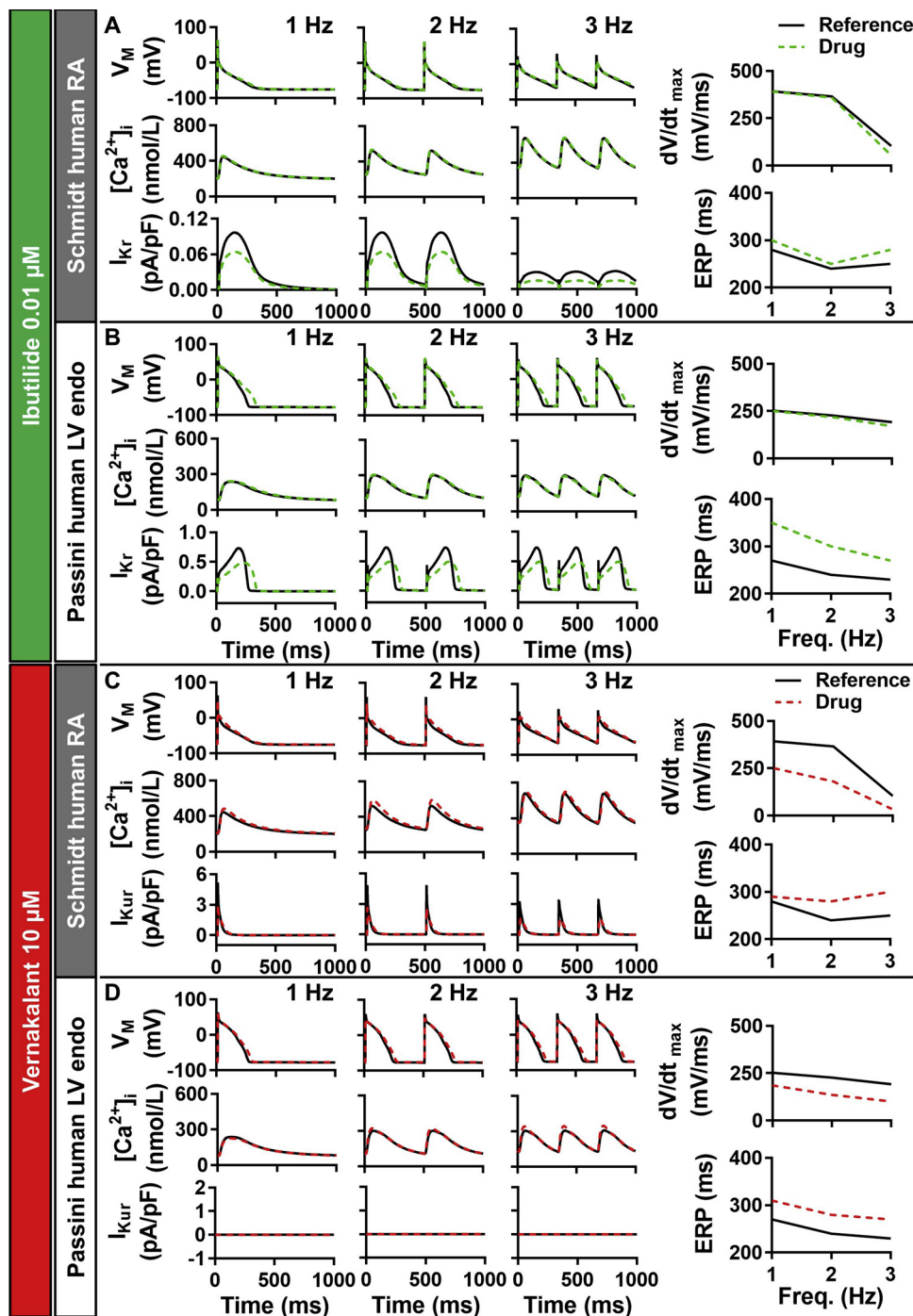


Fig. 5. The effects of ibutilide and vernakalant on upstroke velocity ( $dV/dt_{max}$ ) and effective refractory period (ERP) of human right atrial (RA) and left ventricular (LV) cardiomyocyte models. A–B) Action potentials,  $Ca^{2+}$ -transients and  $I_{Kr}$  during steady-state pacing at 1, 2, or 3 Hz in the absence (black solid lines) or presence (dashed lines) of 0.1  $\mu M$  ibutilide in the Schmidt human RA model (A) and Passini human LV model (B). Rightmost panels show frequency dependence of  $dV/dt_{max}$  and ERP in both models, highlighting a ventricle-predominant effect of ibutilide. C–D) Similar to panels A–D for 10  $\mu M$  vernakalant. In these models, vernakalant exhibits a slight atrial-predominant effect, with larger reduction of  $dV/dt_{max}$  and more ERP prolongation in the human RA model during 3 Hz pacing.

[12,61,62] by blocking  $I_{Kur}$ , which is found exclusively in atrial cardiomyocytes, and favoring inhibition of  $I_{Na}$  at fast rates, as would occur during rapid atrial rhythms like AF. Simulated application of 10  $\mu M$  vernakalant in both atrial and ventricular models at 3 Hz pacing frequency prolonged the ERP by 50 ms and 40 ms, respectively. Similarly, the reduction in maximum upstroke velocity was more pronounced in atrial compared to ventricular cardiomyocyte models (185 mV/ms vs. 91 mV/ms reduction at 2 Hz), suggesting a slight atrial-predominant effect of vernakalant in these models, although this effect was less pronounced than observed experimentally [39,63,64].

### 3.4. Changes in AAD effects in cardiovascular diseases

Cardiovascular diseases such as AF and heart failure produce

extensive ion channel (electrical) remodeling, which may modulate the effect of AADs. For example, all Class III AADs except amiodarone are contraindicated for rhythm control of AF in patients with concomitant heart failure due to increased risk of ventricular proarrhythmia under these conditions [5]. Amiodarone has differential acute and chronic electrophysiological effects (Supplemental Table 1). We compared the steady-state effects of chronic amiodarone, as would be used for long-term rhythm control, dofetilide and sotalol on APD in Passini human LV cardiomyocyte models with and without heart failure-related electrical remodeling, as reported by [65] (Fig. 6). Heart failure-related electrical remodeling resulted in reduced  $I_{Kr}$ , prolonged APD and CaT duration, reduced CaT amplitude, and increased diastolic  $Ca^{2+}$  levels (Fig. 6A and B) [31]. Inhibition of  $I_{Kr}$  by sotalol and dofetilide produced a concentration-dependent increase in APD, which was more pronounced

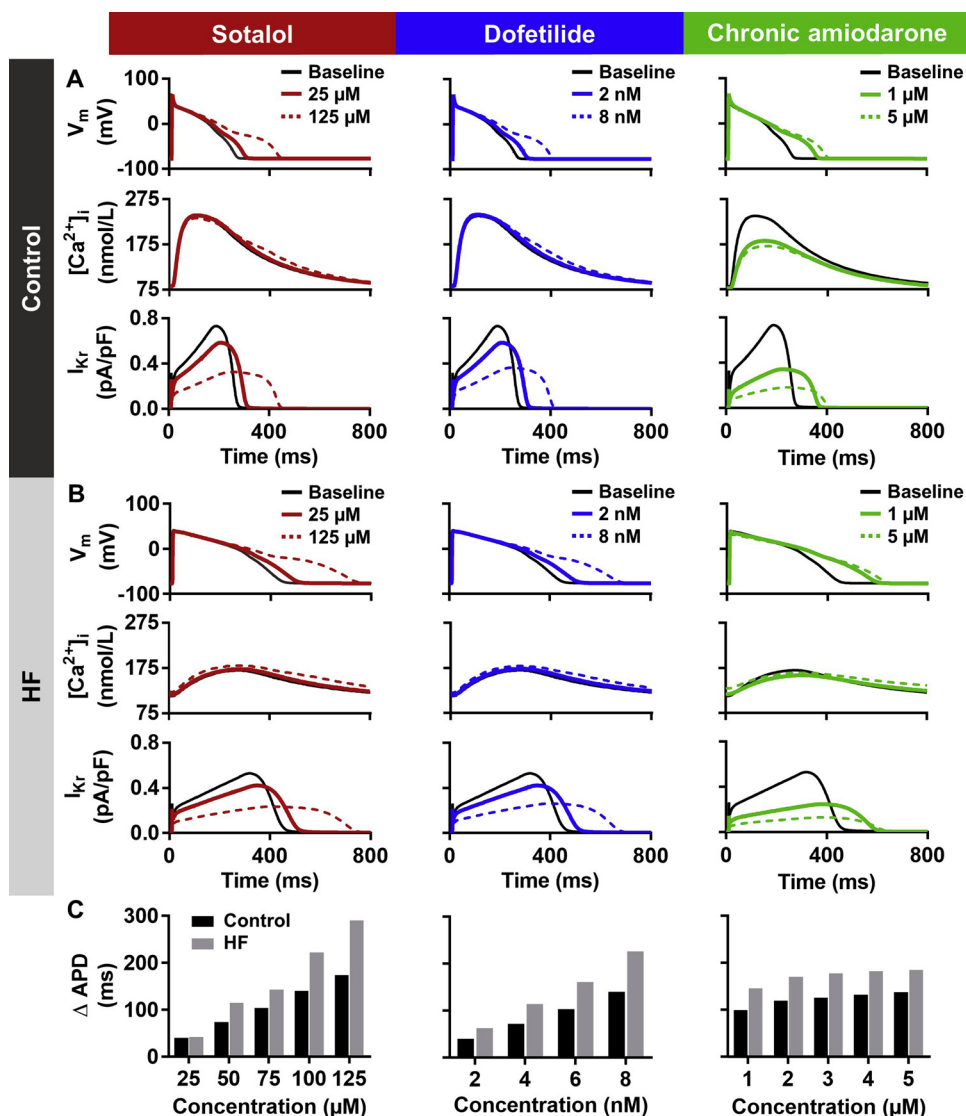


**Fig. 6.** The effects of sotalol, dofetilide and chronic amiodarone on the action potential duration (APD) of Passini human ventricular cardiomyocyte models with or without heart failure (HF)-related electrical remodeling. Degree of HF-related electrical remodeling was based on [65]. A–B) Action potentials,  $\text{Ca}^{2+}$  transients and  $\text{I}_{\text{Kr}}$  in models without (control, A) and with (B) HF-related electrical remodeling in the absence or presence of sotalol, dofetilide or chronic amiodarone (left to right). Sotalol, dofetilide and chronic amiodarone prolonged APD in all models by blocking  $\text{I}_{\text{Kr}}$ . C) Quantification of APD changes induced by various concentrations of sotalol, dofetilide and chronic amiodarone in control (black bars) and HF (grey bars) models. Sotalol and dofetilide produced a more pronounced concentration-dependent APD prolongation in the HF model compared to the control (non-HF) model, which was not observed with chronic amiodarone.

in the heart failure compared to the control model. For example, simulated application of sotalol (125  $\mu\text{M}$ ) resulted in a larger APD prolongation (286 ms) in the heart failure model compared to the control model (169 ms). Similarly, dofetilide (8 nM) prolonged APD by 222 ms and 136 ms in the heart failure and control models, respectively. This excessive concentration-dependent APD prolongation in the setting of heart failure-related remodeling was less pronounced during simulated application of chronic amiodarone (Fig. 6B), consistent with its lower proarrhythmic risk in heart failure patients.

We also employed MANTA to investigate the steady-state electrophysiological effects of AADs in the Schmidt human RA cardiomyocyte model with and without long-standing persistent ('chronic') AF (cAF)-related remodeling (Fig. 7). Simulated application of sotalol during 2 Hz pacing resulted in a similar concentration-dependent prolongation of APD in both the model with and without cAF-related remodeling (18 ms and 53 ms increase with 50  $\mu\text{M}$  or 400  $\mu\text{M}$  sotalol in cAF vs. 19 ms and 47 ms in control). High concentrations of sotalol also reduced  $\text{dV}/\text{dt}_{\text{max}}$  due to inhibition of  $\text{I}_{\text{K1}}$ , leading to depolarization of resting membrane potential, as well as slight  $\text{I}_{\text{Na}}$  inhibition. This effect was less pronounced in the presence of cAF-related remodeling (21 mV/ms vs. 45 mV/ms), which reduces the resting membrane potential. The effects of the Class Ic AAD flecainide also depended on the disease condition. In the model with cAF-related remodeling paced at 2 Hz, APD prolongation was smaller (46 ms and 81 ms increase with 2  $\mu\text{M}$  or

8  $\mu\text{M}$  flecainide, respectively) compared to the control model (53 ms and 95 ms). In addition, the flecainide-induced reduction of  $\text{dV}/\text{dt}_{\text{max}}$  was smaller (11 mV/ms and 35 mV/ms reduction with 2  $\mu\text{M}$  and 8  $\mu\text{M}$  flecainide) compared to the control model (27 mV/ms and 76 mV/ms) due to hyperpolarization of the resting membrane potential, further highlighting the disease-specific effects of AADs. By contrast, simulated application of 0.5  $\mu\text{M}$  chronic amiodarone had similar effects on  $\text{dV}/\text{dt}_{\text{max}}$  in the cAF model and the control model (22 mV/ms reduction), although the APD-prolonging effects at this concentration were minimal. These observations are consistent with *in vivo* measurements in AF patients showing unaltered monophasic APD but reduced intra-atrial conduction velocity in the presence of amiodarone [66], although APD-prolonging effects have also been described [67]. The fact that amiodarone-induced electrophysiological effects are preserved in cAF may contribute to the superior clinical effectiveness of this AAD for long-term rhythm control in AF patients compared to sotalol and flecainide [4].

#### 4. Discussion

Understanding the effect of AADs in the heart can often be challenging yet is needed for better arrhythmia management. In this study, we presented MANTA, a novel computational tool to predict the cellular effects of AADs in various species, regions of the heart and experimental

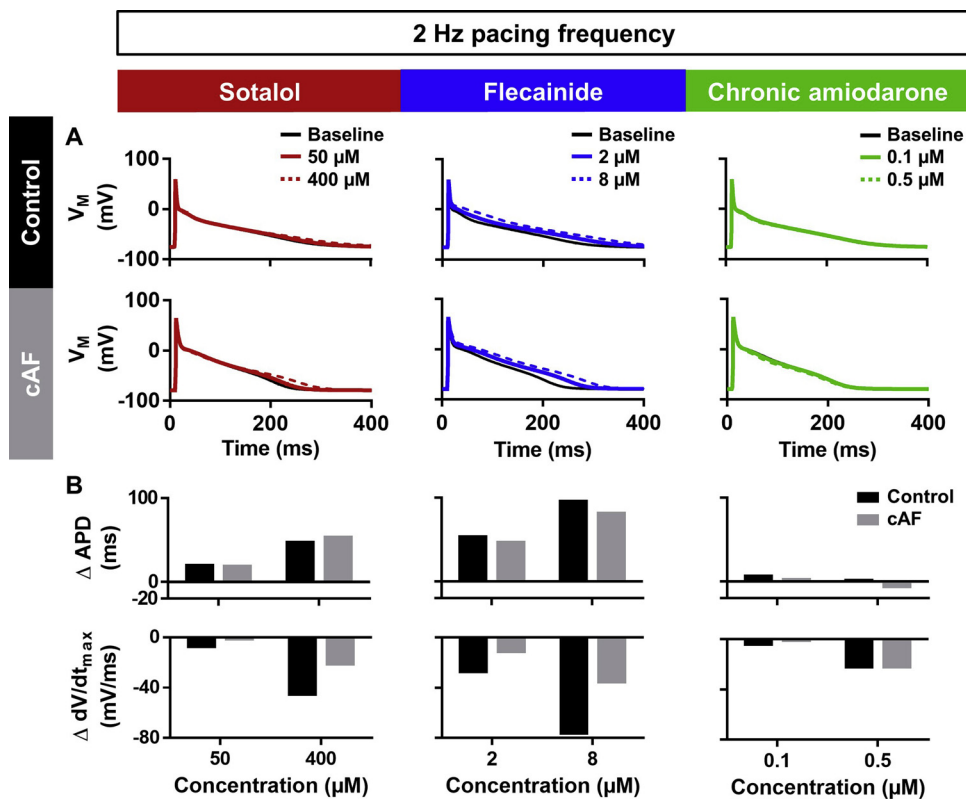


**Fig. 7.** The effects of sotalol, flecainide and chronic amiodarone on action potential (AP) duration (APD) and upstroke velocity ( $dV/dt_{max}$ ) of Schmidt human RA models with and without long-standing persistent ('chronic') atrial fibrillation (cAF)-related electrical remodeling. A) APs at baseline and with 50 and 400  $\mu$ M Sotalol (left), 2 and 8  $\mu$ M flecainide (center) and 0.1 and 0.5  $\mu$ M chronic amiodarone for control (top) and cAF (bottom) cardiomyocyte models. B) Quantification of APD changes compared to baseline (top) and difference in  $dV/dt_{max}$  compared to baseline (bottom) for control (black) and cAF (grey) cardiomyocyte models.

settings. Our simulations reproduce a number of key characteristics: 1) species-specific effects of AADs, 2) rate-dependent effects of AADs, 3) the atrial specificity of vernakalant, and 4) the superiority of chronic amiodarone as an antiarrhythmic therapy in the setting of heart failure and cAF. Our data establish MANTA as a useful tool to analyze the mechanisms underlying a wide range of AAD properties and to illustrate the distinct properties of AADs for educational purposes.

#### 4.1. Diversity of AAD actions

AAD therapy plays a major role in cardiac arrhythmia management but choosing the optimal AAD for an individual patient is highly challenging. Several AADs, including quinidine, flecainide, dofetilide and sotalol can promote ventricular proarrhythmia [57]. Since quinidine was introduced as one of the first AADs more than a century ago [68], significant efforts have therefore been made to develop new AADs with increased efficacy and fewer adverse side-effects. However, progress has been limited, likely in part due to an incomplete understanding of both the underlying arrhythmia mechanisms and complex electrophysiological effects of AADs [69]. Using MANTA, we could demonstrate that AADs have pronounced species-dependent effects, which were due to the differential expression of cardiac ion channels, resulting in distinct APD/ERP prolongation across species [8,70], as well as in different regions of the heart [71,72]. Such species-dependent effects make the selection of appropriate animal models for AAD testing essential. In addition, simulated application of Class I and III AADs resulted in rate-dependent electrophysiological effects due to their (reverse) rate-dependent behavior [11]. Cardiovascular diseases such as AF and heart failure produce abnormalities in cardiac electrophysiology and  $Ca^{2+}$  handling [73–75], which may change the pharmacodynamics of AADs. We demonstrated preserved electrophysiological effects during simulated application of chronic amiodarone in cardiomyocyte models with cAF- or heart failure-related electrical remodeling, illustrating how MANTA can be used to assess disease-specific AAD effects.

Nonetheless, the wide spectrum of comorbidities associated with

these cardiovascular diseases may also affect the pharmacokinetics of AADs, potentially altering drug absorption, metabolism or excretion and making it more difficult to develop AADs with strong efficacy without evoking major adverse events. Together, these complex interactions between AAD properties and actual clinical conditions make it challenging to intuitively predict whether the antiarrhythmic actions of AADs would outweigh their potential proarrhythmic tendencies [10].

AADs with atrial-predominant effects might provide safer options for pharmacological treatment of AF. In general, the atrial specificity of these AADs is achieved by their  $I_{Kur}$  blocking effect, a higher affinity for the inactivated state of the cardiac  $Na^+$ -channel and fast  $Na^+$ -channel dissociation kinetics [76]. Atrial cardiomyocytes have a more depolarized resting membrane potential compared to ventricular cardiomyocytes, particularly at fast rates such as during AF, which promotes the atrial-predominant effect of these AADs [39,64,76]. In agreement, we could demonstrate ventricular-predominant effects of Class III AADs and a slight atrial-predominant effect of simulated vernakalant. Moreover, MANTA makes it easy to adjust the affinity of an AAD for individual targets, enabling investigations of the optimal AAD properties for a given clinical condition, for example to achieve AF-predominant effects.

#### 4.2. Role of computational modeling in cardiac arrhythmia management

In the last few decades, computational modeling of cardiac electrophysiology has contributed to a better understanding of cardiac arrhythmogenesis. Until now, more than 50 computational cardiomyocyte models of different species and regions of the heart have been developed to investigate cardiac electrophysiology and (patho)physiology. Based on these advances, *in silico* modeling has also become a central element in the Comprehensive *in vitro* Proarrhythmia Assay (CiPA) initiative to assess the safety profile of new drugs [77]. For example, the Virtual Assay [22] provides a framework for *in silico* proarrhythmic toxicity trials in a population of calibrated human ventricular cardiomyocyte models and can predict clinical risk of 62

reference compounds with high accuracy. In addition, the U.S. Food and Drug Administration (FDA) aims to transform computational modeling from a scientific tool into a valuable regulatory instrument in which digital evidence is being used instead of other types of evidence [78]. Moreover, whole-heart modeling has recently been employed to support the decision-making process prior to catheter ablation of AF [79]. Thus, several novel clinical and regulatory applications of computational modeling are starting to emerge.

In addition, several educational tools have been developed to teach cardiac (cellular) electrophysiology. For example, LabHEART® provides a user-friendly tool to simulate ion currents and  $\text{Ca}^{2+}$ -transport proteins in a rabbit ventricular myocyte [18], the MioLab® simulator describes  $\text{Ca}^{2+}$  dynamics and contractile forces during contraction and relaxation of cardiomyocytes [19], and the web-based simulation platform eSolv enables teachers to load a cardiomyocyte CellML model and generate simulations adapted to the students' level by defining whether and to what extent model parameters can be changed [20]. Although it is possible to perform simulations with ion-channel blockers in both eSolv and MioLab®, as well as in the more generic cardiomyocyte simulation tools Myokit [23] and LongQt [21], these computational tools are limited in their ability to compare the effects of AADs on the AP under various conditions in a user-friendly way. They do not contain a library of cardiomyocyte models, nor do they come with multiple AADs, which effects can be simulated simultaneously in a reasonably short period of time. Moreover, these tools do not incorporate the state-dependent effects of AADs, which are particularly relevant for Class I AADs. MANTA was developed to facilitate analyses of the cellular effects of currently available AADs under user-defined experimental settings. It also serves as a library of commonly used cardiomyocyte models and AADs, with a capability to simulate the cellular effects of AADs using either state-dependent regulation or  $\text{IC}_{50}$ -based inhibition of cardiac ion channels. MANTA also enables a direct comparison of the effects of two AADs on two different cardiomyocyte models. Finally, MANTA combines these features in a user-friendly interface, so that the users can operate MANTA without extensive guidance and/or modeling skills. As such, MANTA can function as an educational tool to help students understand the cellular mechanism of AADs, as well as their species- and condition-dependent effects. As MANTA facilitates comparison between two AADs under user-defined experimental/environmental settings, including heart rate / pacing frequency and electrolyte concentrations, it enables simulations to dissect, for example, why AADs are contraindicated under certain simulated pathophysiological conditions such as hypo/hyperkalemia or bradycardia.

#### 4.3. Potential limitations

We employed 17 previously published cellular cardiomyocyte models, each with their own limitations, which likely affect the outcome of AAD simulations. For example, the original Luo-Rudy Guinea pig model [25] does not consider different  $\text{K}^{+}$ -channel subtypes, precluding reliable analyses of Class III AADs in this particular model. Similarly, we enable the users to change the extracellular  $[\text{Ca}^{2+}]$ ,  $[\text{K}^{+}]$ , and  $[\text{Na}^{+}]$  to observe the effects of different extracellular ionic concentrations on the AP. However, the effects might not be representative if the range of applicability of a particular model is exceeded, as previously shown by Severi et al [80] for changes in extracellular  $\text{Ca}^{2+}$ . Such model limitations should be considered when interpreting simulation results. On the other hand, the ability to quickly compare drug effects in two models of the same species/region in MANTA may help to highlight such limitations.

We simulated the effects of AADs on individual cardiac ion channels based on previously published experimental  $\text{IC}_{50}$  values, which may be influenced by various experimental conditions, including the cell type, temperature, ionic concentrations and voltage-clamp protocols [81–83]. Indeed, as seen in Supplemental Fig. 1, there are differences

in the reported  $\text{IC}_{50}$  values between studies and the availability of data in human cardiomyocytes is rather limited. As such, some validation of the state-dependent  $\text{I}_{\text{Na}}$  inhibition was adapted from non-human experimental data, which may bias the results. In addition, there is evidence that dynamic state-dependent block may also be relevant for other ion channels (e.g.  $\text{I}_{\text{Kur}}$ ,  $\text{I}_{\text{Kr}}$  and  $\text{I}_{\text{SK}}$ ) [14,84–87], so as more experimental data become available, future work might consider replacing the  $\text{IC}_{50}$ -based inhibition of ion currents with state-dependent inhibition using detailed Markov models. Nevertheless, the cellular electrophysiological response (e.g., APD prolongation) of several AADs and models was consistent with experimental data (Supplemental Fig. 2), strongly suggesting that the current approach provides a reasonable approximation. Finally, in the current version of MANTA, we incorporated drug effects on 10 major cardiac ion currents. However, data about AAD effects on several additional cardiac ion channels is emerging, including the acetylcholine-activated inward-rectifier  $\text{K}^{+}$ -channel and two-pore domain  $\text{K}^{+}$ -channel [33], hyperpolarization-activated cyclic nucleotide-gated (HCN) channel [88], transient receptor potential (TRP) channels [89] and voltage-gated Kv1.1 channels [90], which are not included in most current cardiomyocyte models. Therefore, it is currently not possible to simulate the effect of AADs such as ivabradine [88], BMS914392 [91], NIP-151 [92] and tertiapin [93], which exert their function mainly through those channels. Similarly, the absence of  $\beta$ -adrenoceptor-signaling components in almost all cardiomyocyte models precludes simulation of the effects of Class II AADs and makes it difficult to simulate exercise, which is a well-known proarrhythmic trigger [29,74,94,95], although MANTA allows users to simulate the effects of AADs during higher pacing frequencies.

Importantly, although MANTA can provide useful general information about species- and condition-specific AAD effects, there is pronounced inter-individual variability in cardiac electrophysiology and pharmacokinetics that can influence AAD effects. Although population-based approaches have been proposed to simulate inter-individual variability [22], patient-specific risk assessment or recommendation of AAD therapy is currently not feasible.

#### 4.4. Future outlook and potential contributions of MANTA

We have shown that MANTA can reproduce a large number of clinically relevant AAD characteristics at the cellular level and can be used to investigate the underlying ionic mechanisms. However, various publications have shown that the cellular effects of an AAD can be different from organ-level effects due to cell-to-cell interactions, spatial heterogeneities in electrical properties and additional factors, such as autonomic innervation [7,70,96–98]. Importantly, arrhythmias are inherently tissue-level phenomena and to study pro- or antiarrhythmic actions of AADs the tool would have to be extended to tissue or whole-heart simulations. At present, these simulations are computationally demanding, limiting the educational use of the tool. However, as processor speeds increase, future versions of MANTA may be able to accommodate such simulations, significantly increasing the clinical relevance of the tool.

MANTA simulates the effects of AADs based on a given cellular concentration. At the moment, it is hard to determine the appropriate concentration based on the clinical drug dose due to the different pharmacokinetics of each AAD. Pharmacokinetic models for different cardiovascular drugs have been established that enable simulation of plasma concentrations over time [99,100]. In the future, MANTA could incorporate such pharmacokinetic models to investigate the electrophysiological effects of various dosing strategies for different AADs.

## 5. Conclusions

The effects of AADs are complex and highly dependent on the experimental or clinical conditions. MANTA is a powerful, freely available tool able to reproduce a wide range of AAD characteristics including

species-, rate-, and disease-dependent effects. MANTA enables analyses of the underlying ionic mechanisms as well as investigations of novel AADs with specific affinities for one or more targets. MANTA can facilitate a better understanding of AAD effects on cellular electrophysiology under a wide range of conditions, which may provide educational and/or clinically-relevant information on the safety and efficacy of AAD treatment.

## Funding

The authors' work was supported by grants from the Netherlands Organization for Scientific Research (ZonMW Veni 91616057 to JH), the Biotechnology and Biological Sciences Research Council (BBSRC BB/P010008/1 to MC), the National Institutes of Health (R01-HL131517 and R01-HL136389 to DD), and the German Research Foundation (DFG, Do 769/4-1 to DD).

## Declaration of Competing Interest

The authors declare that the research was conducted in the absence of any commercial or financial relationships that could be construed as a potential conflict of interest.

## Acknowledgement

None.

## Appendix A. Supplementary data

Supplementary material related to this article can be found, in the online version, at doi:<https://doi.org/10.1016/j.phrs.2019.104444>.

## References

- [1] E.J. Benjamin, S.S. Virani, C.W. Callaway, A.M. Chamberlain, A.R. Chang, S. Cheng, S.E. Chiuve, M. Cushman, F.N. Delling, R. Deo, S.D. de Ferranti, J.F. Ferguson, M. Fornage, C. Gillespie, C.R. Isasi, M.C. Jimenez, L.C. Jordan, S.E. Judd, D. Lackland, J.H. Lichtman, L. Lisabeth, S. Liu, C.T. Longenecker, P.L. Lutsey, J.S. Mackey, D.B. Matchar, K. Matsushita, M.E. Mussolino, K. Nasir, M. O'Flaherty, L.P. Palaniappan, A. Pandey, D.K. Pandey, M.J. Reeves, M.D. Ritchey, C.J. Rodriguez, G.A. Roth, W.D. Rosamond, U.K.A. Sampson, G.M. Satou, S.H. Shah, N.L. Spartano, D.L. Tirschwell, C.W. Tsao, J.H. Voeks, J.Z. Willey, J.T. Wilkins, J.H. Wu, H.M. Alger, S.S. Wong, P. Muntner, et al., American heart association council on, C. Prevention statistics, S. Stroke statistics, heart disease and stroke Statistics-2018 update: a report from the american heart association, *Circulation* 137 (12) (2018) e67–e492, <https://doi.org/10.1161/CIR.0000000000000558>.
- [2] A. Burashnikov, C. Antzelevitch, New developments in atrial antiarrhythmic drug therapy, *Nat. Rev. Cardiol.* 7 (3) (2010) 139–148, <https://doi.org/10.1038/nrcardio.2009.245>.
- [3] G.A. Dan, D. Dobrev, Antiarrhythmic drugs for atrial fibrillation: imminent impulses are emerging, *Int. J. Cardiol. Heart Vasc.* 21 (2018) 11–15, <https://doi.org/10.1016/j.ijcha.2018.08.005>.
- [4] C. Lafuente-Lafuente, L. Valembois, J.F. Bergmann, J. Belmin, Antiarrhythmics for maintaining sinus rhythm after cardioversion of atrial fibrillation, *Cochrane Database Syst. Rev.* (3) (2015) CD005049, <https://doi.org/10.1002/14651858.CD005049.pub4>.
- [5] G.A. Dan, A. Martinez-Rubio, S. Agewall, G. Boriani, M. Borggrefe, F. Gaita, I. van Gelder, B. Gorenek, J.C. Kaski, K. Kjeldsen, G.Y.H. Lip, B. Merkely, K. Okumura, J.P. Piccini, T. Potpara, B.K. Poulsen, M. Saba, I. Savellieva, J.L. Tamargo, C. Wolpert, E.S.C.S.D. Group, Antiarrhythmic drugs-clinical use and clinical decision making: a consensus document from the European Heart Rhythm Association (EHRA) and European Society of Cardiology (ESC) Working Group on Cardiovascular Pharmacology, endorsed by the Heart Rhythm Society (HRS), Asia-Pacific Heart Rhythm Society (APHRS) and International Society of Cardiovascular Pharmacotherapy (ISCP), *Europace* 20 (5) (2018) 731–732, <https://doi.org/10.1093/europace/eux373> an.
- [6] J. Heijman, S. Ghezelbash, D. Dobrev, Investigational antiarrhythmic agents: promising drugs in early clinical development, *Expert Opin. Invest. Drugs* 26 (8) (2017) 897–907, <https://doi.org/10.1080/13543784.2017.1353601>.
- [7] M. Lei, L. Wu, D.A. Terrar, C.L. Huang, Modernized classification of cardiac antiarrhythmic drugs, *Circulation* 138 (17) (2018) 1879–1896, <https://doi.org/10.1161/CIRCULATIONAHA.118.035455>.
- [8] C. Antzelevitch, Ionic, molecular, and cellular bases of QT-interval prolongation and torsade de pointes, *Europace* 9 (Suppl. 4) (2007) iv4–15, <https://doi.org/10.1093/europace/eum166>.
- [9] J. Heijman, J.B. Guichard, D. Dobrev, S. Nattel, Translational challenges in atrial fibrillation, *Circ. Res.* 122 (5) (2018) 752–773, <https://doi.org/10.1161/CIRCRESAHA.117.311081>.
- [10] J. Weirich, H. Antoni, Rate-dependence of antiarrhythmic and proarrhythmic properties of class I and class III antiarrhythmic drugs, *Basic Res. Cardiol.* 93 (Suppl. 1) (1998) 125–132.
- [11] L. Barandi, L. Virag, N. Jost, Z. Horvath, I. Koncz, R. Papp, G. Harmati, B. Horvath, N. Szentandassy, T. Banyasz, J. Magyar, A. Zaza, A. Varro, P.P. Nanasi, Reverse rate-dependent changes are determined by baseline action potential duration in mammalian and human ventricular preparations, *Basic Res. Cardiol.* 105 (3) (2010) 315–323, <https://doi.org/10.1007/s00395-009-0082-7>.
- [12] D. Dobrev, S. Nattel, New antiarrhythmic drugs for treatment of atrial fibrillation, *Lancet* 375 (9721) (2010) 1212–1223, [https://doi.org/10.1016/S0140-6736\(10\)60096-7](https://doi.org/10.1016/S0140-6736(10)60096-7).
- [13] J. Heijman, P. Erfanian Abdoust, N. Voigt, S. Nattel, D. Dobrev, Computational models of atrial cellular electrophysiology and calcium handling, and their role in atrial fibrillation, *J. Physiol. (Paris)* 594 (3) (2016) 537–553, <https://doi.org/10.1113/JP271404>.
- [14] E. Grandi, D. Dobrev, J. Heijman, Computational modeling: What does it tell us about atrial fibrillation therapy? *Int. J. Cardiol.* 287 (2019) 155–161, <https://doi.org/10.1016/j.ijcard.2019.01.077>.
- [15] S.A. Niederer, J. Lumens, N.A. Trayanova, Computational models in cardiology, *Nat. Rev. Cardiol.* 16 (2) (2019) 100–111, <https://doi.org/10.1038/s41569-018-0104-y>.
- [16] T. Arts, T. Delhaas, P. Bovendeerd, X. Verbeek, F.W. Prinzen, Adaptation to mechanical load determines shape and properties of heart and circulation: the CircAdapt model, *Am. J. Physiol. Heart Circ. Physiol.* 288 (4) (2005) H1943–54, <https://doi.org/10.1152/ajpheart.00444.2004>.
- [17] A. van Oosterom, T.F. Oostendorp, ECGSIM: an interactive tool for studying the genesis of QRS waveforms, *Heart* 90 (2) (2004) 165–168.
- [18] J.L. Puglisi, D.M. Bers, LabHEART: an interactive computer model of rabbit ventricular myocyte ion channels and Ca transport, *Am. J. Physiol., Cell Physiol.* 281 (6) (2001) C2049–2060, <https://doi.org/10.1152/ajpcell.2001.281.6.C2049>.
- [19] R.R. da Silva, M.A. Bissaco, D.G. Goroso, MioLab, a rat cardiac contractile force simulator: Applications to teaching cardiac cell physiology and biophysics, *Comput. Methods Programs Biomed.* 122 (3) (2015) 480–490, <https://doi.org/10.1016/j.cmpb.2015.09.012>.
- [20] T.P. de Boer, S. van der Werf, B. Hennekam, D.P. Nickerson, A. Garny, M. Gerbrands, R.A.M. Bouwmeester, A.P. Rozendal, E. Torfs, H.V.M. van Rijen, eSolv, a CellML-based simulation front-end for online teaching, *Adv. Physiol. Educ.* 41 (3) (2017) 425–427, <https://doi.org/10.1152/advan.00127.2016>.
- [21] B. Onal, D. Gratz, T. Hund, LongQt: A cardiac electrophysiology simulation platform, *MethodsX* 3 (2016) 589–599, <https://doi.org/10.1016/j.mex.2016.11.002>.
- [22] E. Passini, O.J. Britton, H.R. Lu, J. Rohrbacher, A.N. Hermans, D.J. Gallacher, R.J.H. Greig, A. Bueno-Orovio, B. Rodriguez, Human in silico drug trials demonstrate higher accuracy than animal models in predicting clinical pro-arrhythmic cardiotoxicity, *Front. Physiol.* 8 (2017) 668, <https://doi.org/10.3389/fphys.2017.00668>.
- [23] M. Clerx, P. Collins, E. de Lange, P.G. Volders, Myokit: A simple interface to cardiac cellular electrophysiology, *Prog. Biophys. Mol. Biol.* 120 (1–3) (2016) 100–114, <https://doi.org/10.1016/j.pbiomolbio.2015.12.008>.
- [24] V.E. Bondarenko, G.P. Szegedi, G.C. Bett, S.J. Kim, R.L. Rasmusson, Computer model of action potential of mouse ventricular myocytes, *Am. J. Physiol. Heart Circ. Physiol.* 287 (3) (2004) H1378–403, <https://doi.org/10.1152/ajpheart.00185.2003>.
- [25] C.H. Luo, Y. Rudy, A model of the ventricular cardiac action potential. Depolarization, repolarization, and their interaction, *Circ. Res.* 68 (6) (1991) 1501–1526.
- [26] G.M. Faber, Y. Rudy, Action potential and contractility changes in  $[Na^+]_i$  overloaded cardiac myocytes: a simulation study, *Biophys. J.* 78 (5) (2000) 2392–2404, [https://doi.org/10.1016/S0006-3495\(00\)76783-X](https://doi.org/10.1016/S0006-3495(00)76783-X).
- [27] A. Mahajan, Y. Shiferaw, D. Sato, A. Baher, R. Olcese, L.H. Xie, M.J. Yang, P.S. Chen, J.G. Restrepo, A. Karma, A. Garfinkel, Z. Qu, J.N. Weiss, A rabbit ventricular action potential model replicating cardiac dynamics at rapid heart rates, *Biophys. J.* 94 (2) (2008) 392–410, <https://doi.org/10.1529/biophysj.106.98160>.
- [28] K.F. Decker, J. Heijman, J.R. Silva, T.J. Hund, Y. Rudy, Properties and ionic mechanisms of action potential adaptation, restitution, and accommodation in canine epicardium, *Am. J. Physiol. Heart Circ. Physiol.* 296 (4) (2009) H1017–26, <https://doi.org/10.1152/ajpheart.01216.2008>.
- [29] J. Heijman, P.G. Volders, R.L. Westra, Y. Rudy, Local control of beta-adrenergic stimulation: effects on ventricular myocyte electrophysiology and  $Ca^{2+}$ -transient, *J. Mol. Cell. Cardiol.* 50 (5) (2011) 863–871, <https://doi.org/10.1016/j.jmcc.2011.02.007>.
- [30] T. O'Hara, L. Virag, A. Varro, Y. Rudy, Simulation of the undiseased human cardiac ventricular action potential: model formulation and experimental validation, *PLoS Comput. Biol.* 7 (5) (2011) e1002061, <https://doi.org/10.1371/journal.pcbi.1002061>.
- [31] E. Passini, A. Mincholé, R. Coppini, E. Cerbai, B. Rodriguez, S. Severi, A. Bueno-Orovio, Mechanisms of pro-arrhythmic abnormalities in ventricular repolarisation and anti-arrhythmic therapies in human hypertrophic cardiomyopathy, *J. Mol. Cell. Cardiol.* 96 (2016) 72–81, <https://doi.org/10.1016/j.jmcc.2015.09.003>.
- [32] M. Courtemanche, R.J. Ramirez, S. Nattel, Ionic mechanisms underlying human atrial action potential properties: insights from a mathematical model, *Am. J. Physiol.* 275 (1 Pt 2) (1998) H301–21.
- [33] C. Schmidt, F. Wiedmann, N. Voigt, X.B. Zhou, J. Heijman, S. Lang, V. Albert, S. Kallenberger, A. Ruhparwar, G. Szabo, K. Kallenbach, M. Karck, M. Borggrefe,

- P. Biliczki, J.R. Ehrlich, I. Baczkó, P. Lugenbiel, P.A. Schweizer, B.C. Donner, H.A. Katus, D. Dobrev, D. Thomas, Upregulation of  $K(2P)3.1 K^+$  Current Causes Action Potential Shortening in Patients With Chronic Atrial Fibrillation, *Circulation* 132 (2) (2015) 82–92, <https://doi.org/10.1161/CIRCULATIONAHA.114.012657>.
- [34] P. Stewart, O.V. Aslanidi, D. Noble, P.J. Noble, M.R. Boyett, H. Zhang, Mathematical models of the electrical action potential of Purkinje fibre cells, *Philos. Trans. A Math. Phys. Eng. Sci.* 367 (2009) 2225–2255, <https://doi.org/10.1098/rsta.2008.0283>.
- [35] K.J. Sampson, V. Iyer, A.R. Marks, R.S. Kass, A computational model of Purkinje fibre single cell electrophysiology: implications for the long QT syndrome, *J. Physiol. (Paris)* 588 (Pt 14) (2010) 2643–2655, <https://doi.org/10.1113/jphysiol.2010.187328>.
- [36] J.D. Moreno, Z.I. Zhu, P.C. Yang, J.R. Bankston, M.T. Jeng, C. Kang, L. Wang, J.D. Bayer, D.J. Christini, N.A. Trayanova, C.M. Ripplinger, R.S. Kass, C.E. Clancy, A computational model to predict the effects of class I anti-arrhythmic drugs on ventricular rhythms, *Sci. Transl. Med.* 3 (98) (2011) 98ra83, <https://doi.org/10.1126/scitranslmed.3002588>.
- [37] L.M. Hondeghem, B.G. Katzung, Antiarrhythmic agents: the modulated receptor mechanism of action of sodium and calcium channel-blocking drugs, *Annu. Rev. Pharmacol. Toxicol.* 24 (1984) 387–423, <https://doi.org/10.1146/annurev.pa.24.040184.002131>.
- [38] J.R. Balser, The cardiac sodium channel: gating function and molecular pharmacology, *J. Mol. Cell. Cardiol.* 33 (4) (2001) 599–613, <https://doi.org/10.1006/jmcc.2000.1346>.
- [39] D. Fedida, P.M. Orth, J.Y. Chen, S. Lin, B. Plouvier, G. Jung, A.M. Ezrin, G.N. Beatch, The mechanism of atrial antiarrhythmic action of RSD1235, *J. Cardiovasc. Electrophysiol.* 16 (11) (2005) 1227–1238, <https://doi.org/10.1111/j.1540-8167.2005.50028.x>.
- [40] J. Heijman, V. Algalarrondo, N. Voigt, J. Melka, X.H. Wehrens, D. Dobrev, S. Nattel, The value of basic research insights into atrial fibrillation mechanisms as a guide to therapeutic innovation: a critical analysis, *Cardiovasc. Res.* 109 (4) (2016) 467–479, <https://doi.org/10.1093/cvr/cvv275>.
- [41] C.A. Obejero-Paz, A. Bruening-Wright, J. Kramer, P. Hawryluk, M. Tatalovic, H.C. Dittrich, A.M. Brown, Quantitative profiling of the effects of Vanoxerine on human cardiac ion channels and its application to cardiac risk, *Sci. Rep.* 5 (2015) 17623, <https://doi.org/10.1038/srep17623>.
- [42] W.J. Crumb Jr., J. Vicente, L. Johannesen, D.G. Strauss, An evaluation of 30 clinical drugs against the comprehensive in vitro proarrhythmia assay (CiPA) proposed ion channel panel, *J. Pharmacol. Toxicol. Methods* 81 (2016) 251–262, <https://doi.org/10.1016/j.vascn.2016.03.009>.
- [43] A.R. Harmer, J.P. Valentin, C.E. Pollard, On the relationship between block of the cardiac  $Na^+$  channel and drug-induced prolongation of the QRS complex, *Br. J. Pharmacol.* 164 (2) (2011) 260–273, <https://doi.org/10.1111/j.1476-5381.2011.01415.x>.
- [44] J. Kramer, C.A. Obejero-Paz, G. Myatt, Y.A. Kuryshv, A. Bruening-Wright, J.S. Verducci, A.M. Brown, MICE models: superior to the HERG model in predicting Torsade de Pointes, *Sci. Rep.* 3 (2013) 2100, <https://doi.org/10.1038/srep02100>.
- [45] S. Zhang, Z. Zhou, Q. Gong, J.C. Makielski, C.T. January, Mechanism of block and identification of the verapamil binding domain to HERG potassium channels, *Circ. Res.* 84 (9) (1999) 989–998.
- [46] G.R. Mirams, Y. Cui, A. Sher, M. Fink, J. Cooper, B.M. Heath, N.C. McMahon, D.J. Gavaghan, D. Noble, Simulation of multiple ion channel block provides improved early prediction of compounds' clinical torsadogenic risk, *Cardiovasc. Res.* 91 (1) (2011) 53–61, <https://doi.org/10.1093/cvr/cvr044>.
- [47] S. Matsuoka, T. Nawada, I. Hisatome, Y. Miyamoto, J. Hasegawa, H. Kotake, H. Mashiba, Comparison of  $Ca^{2+}$  channel inhibitory effects of cibenzone with verapamil on guinea-pig heart, *Gen. Pharmacol.* 22 (1) (1991) 87–91.
- [48] L. Yue, J.L. Feng, Z. Wang, S. Nattel, Effects of ambasilide, quinidine, flecainide and verapamil on ultra-rapid delayed rectifier potassium currents in canine atrial myocytes, *Cardiovasc. Res.* 46 (1) (2000) 151–161.
- [49] H.M. Himmel, A. Busse, M. Hoffmann, R. Beckmann, H. Lohmann, M. Schmidt, E. Wettwer, Field and action potential recordings in heart slices: correlation with established in vitro and in vivo models, *Br. J. Pharmacol.* 166 (1) (2012) 276–296, <https://doi.org/10.1111/j.1476-5381.2011.01775.x>.
- [50] T. Anno, L.M. Hondeghem, Interactions of flecainide with guinea pig cardiac sodium channels. Importance of activation unblocking to the voltage dependence of recovery, *Circ. Res.* 66 (3) (1990) 789–803.
- [51] E. Ramos, M. O'Leary, State-dependent trapping of flecainide in the cardiac sodium channel, *J. Physiol. (Paris)* 560 (Pt 1) (2004) 37–49, <https://doi.org/10.1113/jphysiol.2004.065003>.
- [52] A.O. Peralta, R.M. John, W.H. Gaasch, P.I. Taggart, D.T. Martin, F.J. Venditti, The class III antiarrhythmic effect of sotalol exerts a reverse use-dependent positive inotropic effect in the intact canine heart, *J. Am. Coll. Cardiol.* 36 (4) (2000) 1404–1410.
- [53] M. Rocchetti, A. Besana, G.B. Gurrola, L.D. Possani, A. Zaza, Rate dependency of delayed rectifier currents during the guinea-pig ventricular action potential, *J. Physiol. (Paris)* 534 (Pt 3) (2001) 721–732.
- [54] N.K. Jurkiewicz, M.C. Sanguinetti, Rate-dependent prolongation of cardiac action potentials by a methanesulfonanilide class III antiarrhythmic agent. Specific block of rapidly activating delayed rectifier  $K^+$  current by dofetilide, *Circ. Res.* 72 (1) (1993) 75–83.
- [55] T. Yang, D.M. Roden, Extracellular potassium modulation of drug block of IKr. Implications for torsade de pointes and reverse use-dependence, *Circulation* 93 (3) (1996) 407–411.
- [56] T. Banyasz, B. Horvath, L. Virag, L. Barandi, N. Szentandrassy, G. Harmati, J. Magyar, S. Marangoni, A. Zaza, A. Varro, P.P. Nanasi, Reverse rate dependency is an intrinsic property of canine cardiac preparations, *Cardiovasc. Res.* 84 (2) (2009) 237–244, <https://doi.org/10.1093/cvr/cvp213>.
- [57] P. Kirchhof, S. Benussi, D. Kotecha, A. Ahlsson, D. Atar, B. Casadei, M. Castella, H.C. Diener, H. Heidbuchel, J. Hendricks, G. Hindricks, A.S. Manolis, J. Oldgren, B.A. Popescu, U. Schotten, B. Van Putte, P. Vardas, S. Agewall, J. Camm, G. Baron Esquivias, W. Budts, S. Carerj, F. Casselman, A. Coca, R. De Caterina, S. Deftereos, D. Dobrev, J.M. Ferro, G. Filippatos, D. Fitzsimons, B. Gorenek, M. Guenoun, S.H. Hohnloser, P. Kolh, G.Y. Lip, A. Manolis, J. McMurray, P. Ponikowski, R. Rosenhek, F. Ruschitzka, I. Savelieva, S. Sharma, P. Suwalaki, J.L. Tamargo, C.J. Taylor, I.C. Van Gelder, A.A. Voors, S. Windecker, J.L. Zamorano, K. Zeppenfeld, ESC Guidelines for the management of atrial fibrillation developed in collaboration with EACTS, *Europace* 18 (11) (2016) 1609–1678, <https://doi.org/10.1093/europace/euw295> 2016.
- [58] C.T. January, L.S. Wann, J.S. Alpert, H. Calkins, J.E. Cigarroa, J.C. Cleveland Jr., J.B. Conti, P.T. Ellinor, M.D. Ezekowitz, M.E. Field, K.T. Murray, R.L. Sacco, W.G. Stevenson, P.J. Tchou, C.M. Tracy, C.W. Yancy, A.A.T.F. Members, AHA/ACC/HRS guideline for the management of patients with atrial fibrillation: executive summary: a report of the American College of Cardiology/American Heart Association Task Force on practice guidelines and the Heart Rhythm Society, *Circulation* 130 (23) (2014) 2071–2104, <https://doi.org/10.1161/CIR.0000000000000040> 2014.
- [59] T.Y. Chang, J.N. Liao, T.F. Chao, J.J. Viceria, C.Y. Lin, T.C. Tuan, Y.J. Lin, S.L. Chang, L.W. Lo, Y.F. Hu, F.P. Chung, S.A. Chen, Oral anticoagulant use for stroke prevention in atrial fibrillation patients with difficult scenarios, *Int. J. Cardiol. Heart Vasc.* 20 (2018) 56–62, <https://doi.org/10.1016/j.ijcha.2018.08.003>.
- [60] E.K. Heist, J.N. Ruskin, Drug-induced arrhythmia, *Circulation* 122 (14) (2010) 1426–1435, <https://doi.org/10.1161/CIRCULATIONAHA.109.894725>.
- [61] J. Eldstrom, Z. Wang, H. Xu, M. Pourrier, A. Ezrin, K. Gibson, D. Fedida, The molecular basis of high-affinity binding of the antiarrhythmic compound vernakalant (RSD1235) to Kv1.5 channels, *Mol. Pharmacol.* 72 (6) (2007) 1522–1534, <https://doi.org/10.1124/mol.107.039388>.
- [62] I. Savelieva, R. Graydon, A.J. Camm, Pharmacological cardioversion of atrial fibrillation with vernakalant: evidence in support of the ESC Guidelines, *Europace* 16 (2) (2014) 162–173, <https://doi.org/10.1093/europace/eut274>.
- [63] E. Wettwer, T. Christ, S. Endig, N. Rozmaritsa, K. Matschke, J.J. Lynch, M. Pourrier, J.K. Gibson, D. Fedida, M. Knaut, U. Ravens, The new antiarrhythmic drug vernakalant: ex vivo study of human atrial tissue from sinus rhythm and chronic atrial fibrillation, *Cardiovasc. Res.* 98 (1) (2013) 145–154, <https://doi.org/10.1093/cvr/cvt006>.
- [64] A. Burashnikov, M. Pourrier, J.K. Gibson, J.J. Lynch, C. Antzelevitch, Rate-dependent effects of vernakalant in the isolated non-remodeled canine left atria are primarily due to block of the sodium channel: comparison with ranolazine and di-sotalol, *Circ. Arrhythm. Electrophysiol.* 5 (2) (2012) 400–408, <https://doi.org/10.1161/CIRCEP.111.968305>.
- [65] M.M. Elsharif, P. Shi, E.M. Cherry, Representing variability and transmural differences in a model of human heart failure, *IEEE J. Biomed. Health Inform.* 19 (4) (2015) 1308–1320, <https://doi.org/10.1109/JBHI.2015.2442833>.
- [66] N. Sasaki, I. Watanabe, R. Kogawa, K. Sonoda, K. Takahashi, Y. Okumura, K. Ohkubo, T. Nakai, A. Hirayama, Effects of intravenous amiodarone and ibutilide on action potential duration and atrial conduction kinetics in patients with persistent atrial fibrillation, *Int. Heart J.* 55 (3) (2014) 244–248.
- [67] K. Shinagawa, A. Shiroshita-Takeshita, G. Schram, S. Nattel, Effects of antiarrhythmic drugs on fibrillation in the remodeled atrium: insights into the mechanism of the superior efficacy of amiodarone, *Circulation* 107 (10) (2003) 1440–1446.
- [68] M.J. Walker, Antiarrhythmic drug research, *Br. J. Pharmacol.* 147 (Suppl. 1) (2006) S222–231, <https://doi.org/10.1038/sj.bjp.0706500>.
- [69] A. Goette, G. Hindricks, N. Dagres, J.-C. Deharo, D. Dobrev, R. Hatala, S.H. Hohnloser, C. Leclercq, T. Lewalter, G.Y.H. Lip, J.L. Merino, F. Prinzen, A. Proclemer, H. Pürerfellner, R. Schilling, J. Steffel, I.C. van Gelder, K. Zeppenfeld, I. Zupan, H. Heidbüchel, A. Auricchio, G. Boriani, F. Braunschweig, J.B. Terradellas, L. Mont, H. Burri, A.J. Camm, I. Savelieva, H. Crijns, EHRA White Paper: Knowledge Gaps in Arrhythmia Management—status 2019, (2019), <https://doi.org/10.1093/europace/euz055>.
- [70] J.D. Moreno, C.E. Clancy, Using computational modeling to predict arrhythmogenesis and antiarrhythmic therapy, *Drug Discov. Today Dis. Models* 6 (3) (2009) 71–84, <https://doi.org/10.1016/j.ddmod.2010.03.001>.
- [71] D.C. Bartos, E. Grandi, C.M. Ripplinger, Ion channels in the heart, *Compr. Physiol.* 5 (3) (2015) 1423–1464, <https://doi.org/10.1002/cphy.c140069>.
- [72] N. Chiamvimonvat, Y. Chen-Izu, C.E. Clancy, I. Deschenes, D. Dobrev, J. Heijman, L. Izu, Z. Qu, C.M. Ripplinger, J.I. Vandenberg, J.N. Weiss, G. Koren, T. Banyasz, E. Grandi, M.C. Sanguinetti, D.M. Bers, J.M. Nerbonne, Potassium currents in the heart: functional roles in repolarization, arrhythmia and therapeutics, *J. Physiol. (Paris)* 595 (7) (2017) 2229–2252, <https://doi.org/10.1113/JP272883>.
- [73] N. Voigt, J. Heijman, Q. Wang, D.Y. Chiang, N. Li, M. Karck, X.H.T. Wehrens, S. Nattel, D. Dobrev, Cellular and molecular mechanisms of atrial arrhythmogenesis in patients with paroxysmal atrial fibrillation, *Circulation* 129 (2) (2014) 145–156, <https://doi.org/10.1161/CIRCULATIONAHA.113.006641>.
- [74] D.M. Johnson, G. Antoons, Arrhythmogenic mechanisms in heart failure: linking beta-adrenergic stimulation, stretch, and calcium, *Front. Physiol.* 9 (2018) 1453, <https://doi.org/10.3389/fphys.2018.01453>.
- [75] C.E. Molina, I.H. Abu-Taha, Q. Wang, E. Rosello-Diez, M. Kamler, S. Nattel, U. Ravens, X.H.T. Wehrens, L. Hove-Madsen, J. Heijman, D. Dobrev, Profibrotic, Electrical, and Calcium-Handling Remodeling of the Atria in Heart Failure Patients With and Without Atrial Fibrillation, *Front. Physiol.* 9 (2018) 1383, <https://doi.org/10.3389/fphys.2018.01383>.

- [76] M. Grunnet, B.H. Bentzen, U.S. Sorensen, J.G. Diness, Cardiac ion channels and mechanisms for protection against atrial fibrillation, *Rev. Physiol. Biochem. Pharmacol.* 162 (2012) 1–58, [https://doi.org/10.1007/112\\_2011\\_3](https://doi.org/10.1007/112_2011_3).
- [77] B. Christophe, W.J. Crumb Jr., Impact of disease state on arrhythmic event detection by action potential modelling in cardiac safety pharmacology, *J. Pharmacol. Toxicol. Methods* 96 (2018) 15–26, <https://doi.org/10.1016/j.vascn.2018.12.004>.
- [78] T.M. Morrison, P. Pathmanathan, M. Adwan, E. Margerrison, Advancing regulatory science with computational modeling for medical devices at the FDA's office of science and engineering laboratories, *Front. Med. (Lausanne)* 5 (2018) 241, <https://doi.org/10.3389/fmed.2018.00241>.
- [79] P.M. Boyle, J.B. Hakim, S. Zahid, W.H. Franceschi, M.J. Murphy, A. Prakosa, K.N. Aronis, T. Zghaib, M. Balouch, E.G. Ipek, J. Chrispin, R.D. Berger, H. Ashikaga, J.E. Marine, H. Calkins, S. Nazarian, D.D. Spragg, N.A. Trayanova, The fibrotic substrate in persistent atrial fibrillation patients: comparison between predictions from computational modeling and measurements from focal impulse and rotor mapping, *Front. Physiol.* 9 (2018) 1151, <https://doi.org/10.3389/fphys.2018.01151>.
- [80] S. Severi, C. Corsi, E. Cerbai, From in vivo plasma composition to in vitro cardiac electrophysiology and in silico virtual heart: the extracellular calcium enigma, *Philos. Trans. A Math. Phys. Eng. Sci.* 367 (2009) (1896) 2203–2223, <https://doi.org/10.1098/rsta.2009.0032>.
- [81] J.I. Vandenberg, A. Varghese, Y. Lu, J.A. Bursill, M.P. Mahaut-Smith, C.L. Huang, Temperature dependence of human ether-a-go-go-related gene K<sup>+</sup> currents, *Am. J. Physiol., Cell Physiol.* 291 (1) (2006) C165–175, <https://doi.org/10.1152/ajpcell.00596.2005>.
- [82] Z. Li, S. Dutta, J. Sheng, P.N. Tran, W. Wu, T. Colatsky, A temperature-dependent in silico model of the human ether-a-go-go-related (hERG) gene channel, *J. Pharmacol. Toxicol. Methods* 81 (2016) 233–239, <https://doi.org/10.1016/j.vascn.2016.05.005>.
- [83] C. Lin, I. Cvetanovic, X. Ke, V. Ranade, J. Somberg, A mechanism for the potential proarrhythmic effect of acidosis, bradycardia, and hypokalemia on the blockade of human ether-a-go-go-related gene (HERG) channels, *Am. J. Ther.* 12 (4) (2005) 328–336.
- [84] N. Ellinwood, D. Dobrev, S. Morotti, E. Grandi, In silico assessment of efficacy and safety of I<sub>Kur</sub> inhibitors in chronic atrial fibrillation: role of kinetics and state-dependence of drug binding, *Front. Pharmacol.* 8 (2017) 799, <https://doi.org/10.3389/fphar.2017.00799>.
- [85] Z. Li, S. Dutta, J. Sheng, P.N. Tran, W. Wu, K. Chang, T. Mdluli, D.G. Strauss, T. Colatsky, Improving the in silico assessment of proarrhythmia risk by combining hERG (Human Ether-a-go-go-Related gene) channel-drug binding kinetics and multichannel pharmacology, *Circ. Arrhythm. Electrophysiol.* 10 (2) (2017), <https://doi.org/10.1161/CIRCEP.116.004628> e004628.
- [86] N. Ellinwood, D. Dobrev, S. Morotti, E. Grandi, Revealing kinetics and state-dependent binding properties of I<sub>Kur</sub>-targeting drugs that maximize atrial fibrillation selectivity, *Chaos* 27 (9) (2017) 093918, <https://doi.org/10.1063/1.5000226>.
- [87] M. Vagos, I.G.M. van Herck, J. Sundnes, H.J. Arevalo, A.G. Edwards, J.T. Koivumaki, Computational modeling of electrophysiology and pharmacotherapy of atrial fibrillation: recent advances and future challenges, *Front. Physiol.* 9 (2018) 1221, <https://doi.org/10.3389/fphys.2018.01221>.
- [88] F. Roubille, J.C. Tardif, New therapeutic targets in cardiology: heart failure and arrhythmia: HCN channels, *Circulation* 127 (19) (2013) 1986–1996, <https://doi.org/10.1161/CIRCULATIONAHA.112.000145>.
- [89] H. Watanabe, M. Murakami, T. Ohba, Y. Takahashi, H. Ito, TRP channel and cardiovascular disease, *Pharmacol. Ther.* 118 (3) (2008) 337–351, <https://doi.org/10.1016/j.pharmthera.2008.03.008>.
- [90] E. Glasscock, N. Voigt, M.D. McCauley, Q. Sun, N. Li, D.Y. Chiang, X.B. Zhou, C.E. Molina, D. Thomas, C. Schmidt, D.G. Skapura, J.L. Noebels, D. Dobrev, X.H. Wehrens, Expression and function of Kv1.1 potassium channels in human atria from patients with atrial fibrillation, *Basic Res. Cardiol.* 110 (5) (2015) 505, <https://doi.org/10.1007/s00395-015-0505-6>.
- [91] U. Ravens, Atrial-selective K<sup>+</sup> channel blockers: potential antiarrhythmic drugs in atrial fibrillation? *Can. J. Physiol. Pharmacol.* 95 (11) (2017) 1313–1318, <https://doi.org/10.1139/cjpp-2017-0024>.
- [92] N. Hashimoto, T. Yamashita, N. Tsuruzoe, Characterization of in vivo and in vitro electrophysiological and antiarrhythmic effects of a novel I<sub>KACH</sub> blocker, NIP-151: a comparison with an I<sub>Kr</sub>-blocker dofetilide, *J. Cardiovasc. Pharmacol.* 51 (2) (2008) 162–169.
- [93] J.R. Ehrlich, S. Nattel, Atrial-selective pharmacological therapy for atrial fibrillation: hype or hope? *Curr. Opin. Cardiol.* 24 (1) (2009) 50–55.
- [94] D. Linz, A.D. Elliott, M. Hohl, V. Malik, U. Schotten, D. Dobrev, S. Nattel, M. Bohm, J. Floras, D.H. Lau, P. Sanders, Role of autonomic nervous system in atrial fibrillation, *Int. J. Cardiol.* 15 (287) (2018) 181–188, <https://doi.org/10.1016/j.ijcard.2018.11.091>.
- [95] E. Guasch, B. Benito, X. Qi, C. Cifelli, P. Naud, Y. Shi, A. Mighiu, J.C. Tardif, A. Tadevosyan, Y. Chen, M.A. Gillis, Y.K. Iwasaki, D. Dobrev, L. Mont, S. Heximer, S. Nattel, Atrial fibrillation promotion by endurance exercise: demonstration and mechanistic exploration in an animal model, *J. Am. Coll. Cardiol.* 62 (1) (2013) 68–77, <https://doi.org/10.1016/j.jacc.2013.01.091>.
- [96] D.G. Wenzel, J.W. Kleoppel, Arrhythmias induced by changing the medium of cultured rat heart muscle cells: a model for assessment of antiarrhythmic agents, *J. Pharmacol. Methods* 1 (3) (1978) 269–276.
- [97] G. Members of the Sicilian, New approaches to antiarrhythmic therapy: emerging therapeutic applications of the cell biology of cardiac arrhythmias(1), *Cardiovasc. Res.* 52 (3) (2001) 345–360.
- [98] C.E. Molina, J. Heijman, D. Dobrev, Differences in left versus right ventricular electrophysiological properties in cardiac dysfunction and arrhythmogenesis, *Arrhythm. Electrophysiol. Rev.* 5 (1) (2016) 14–19, <https://doi.org/10.15420/aer.2016.8.2>.
- [99] S.K. Woo, W.K. Kang, K.I. Kwon, Pharmacokinetic and pharmacodynamic modeling of the antiplatelet and cardiovascular effects of cilostazol in healthy humans, *Clin. Pharmacol. Ther.* 71 (4) (2002) 246–252, <https://doi.org/10.1067/mcp.2002.122474>.
- [100] Z. Tylutki, S. Polak, A four-compartment PBPK heart model accounting for cardiac metabolism - model development and application, *Sci. Rep.* 7 (2017) 39494, <https://doi.org/10.1038/srep39494>.